ABSTRACT

Title of Thesis:	A STUDY OF COOL DIFFUSION FLAMES UTILIZING IGNITION DELAY CHARACTERISTICS OF N-HEPTANE AUTOIGNITION SIMULATIONS
	Shubham Pimple, Master of Science, 2024
Thesis Directed By:	Professor Peter B. Sunderland, Department of Fire Protection Engineering

Gaining deeper insights into cool diffusion flames (CDFs) can significantly enhance engine efficiency and reduce emissions, while also filling in knowledge gaps relating to explosion initiation and the transition from smoldering to flaming fires. While detailed computational fluid dynamic (CFD) models can simulate CDFs, they require substantial computational resources due to the need for detailed chemistry and transport resolution. To circumvent these challenges, this study utilizes an alternative approach using Cantera autoignition simulations, which presumes isobaric, adiabatic conditions. The fuel, *n*-heptane, is analyzed through six kinetic mechanisms that capture the spectrum of low and high temperature chemistry. The observed ignition process – manifesting as single, two, or three-stage ignition – is observed to vary with initial conditions. Analysis of ignition delay times unveils the Negative Temperature Coefficient (NTC) behavior, crucial for the existence of stable cool flames. The critical transition temperatures, such as the lower and upper turnover and the crossover temperature are also identified, along with the key chemical species produced during the two-stage ignition process. The peak temperature range for

stoichiometric *n*-heptane CDFs is determined to be between 653 and 804 K, aligning favorably with previous experimental measurements. While the first-stage ignition delay time remains nearly constant, the second-stage ignition delay time noticeably decreases as the mixture becomes richer, up to an equivalence ratio of 32. This reduction is attributed to the rapid temperature increase caused by a larger fuel quantity, which accelerates high-temperature chemical reactions. The NTC temperature range is also seen to shorten as the mixture composition gets richer. While the six chemical kinetic models examined concur about the existence of an NTC regime, variations are observed in the threshold temperatures. The insights gained from this study enhance the understanding of CDFs, setting a foundation for future research into different fuels and varying conditions.

A STUDY OF COOL DIFFUSION FLAMES UTILIZING IGNITION DELAY CHARACTERISITCS OF N-HEPTANE AUTOIGNITION SIMULATIONS

by

Shubham Pimple

Thesis submitted to the Faculty of the Graduate School of the
University of Maryland, College Park, in partial fulfillment
of the requirements for the degree of
Master of Science
2024

Advisory Committee:
Professor Peter B. Sunderland, Chair
Professor Emeritus James Milke
Professor Arnaud Trouvé

Acknowledgements

First of all, I would like to express my deepest gratitude to my advisor. Thank you, Dr. Peter Sunderland, for your patience and support throughout the project. Your continued encouragement and belief in me gave me the confidence to lead this work to what it is today. Beyond the valuable knowledge and research experience you have given me, you have also taught me invaluable lessons about quality, kindness, work ethic, communication, among many other virtues.

I am grateful to Dr. Vedha Nayagam at Case Western Reserve University for providing me with a clear direction and guidance for the project.

Next, I would like to thank Dr. Arnaud Trouvé and Dr. James Milke for being on my advisory committee. Their insightful feedback has been incredibly beneficial. The lessons learned from their courses and the TA experiences they provided have been invaluable, as has their guidance throughout my journey in the department.

I would also like to express my heartfelt gratitude to the faculty and staff of the Department of Fire Protection Engineering for supporting me. I would also like to thank the National Science Foundation for funding this study.

Finally, I would like to thank my family for their steadfast support and belief in my abilities. Embarking to a foreign country to fulfil a dream comes with its set of difficulties, but my family's love and backing have been the true pillars of my strength. Furthermore, I deeply appreciate the unwavering friendship and support offered by Saleel Anthrathodiyil, as well as the motivation and valuable experiences shared with me by Zishanul Hussain and Deepanshu Bhatia throughout my graduate studies.

Table of Contents

List of Figures

List of Tables

List of Abbreviations

AIT	Autoignition Temperature
CALTECH	California Institute of Technology
CDF	Cool Diffusion Flame
CERFACS	Center For Research and Advanced Training in Scientific Computing
CI	Compression Ignition
CN	Cetane Number
CO	Carbon Monoxide
CO_2	Carbon Dioxide
H_2O	Water
H_2O_2	Hydrogen Peroxide
HC	Hydrocarbon
HCCI	Homogenous Charge Compression Ignition
HO_2	Hydroperoxy Radical
HT	High Temperature
HTC	High Temperature Chemistry
HTI	High Temperature Ignition
IC	Internal Combustion
IDT	Ignition Delay Time
ISS	International Space Station
ITC	Intermediate Temperature Chemistry
KHP	Keto-hydroperoxide
LLNL	Lawrence Livermore National Laboratories
LT	Low Temperature
LTC	Low Temperature Chemistry
LTI	Low Temperature Ignition
C_7H_{16}	Heptane
NTC	Negative – Temperature Coefficient

NUIG	National University of Ireland Galway
OH	Hydroxyl Ion
PCCI	Premixed Charge Compression Ignition
PM	Particulate Matter
PRF	Primary Reference Fuel
RCCI	Reactivity-Controlled Compression Ignition
RCMs	Rapid Compression Machines
SI	Spark Ignition
U.S.	United States
UCSD	University Of California San Diego

Chapter 1: Introduction

Even with the advances made in renewable energy technologies, global energy production continues to rely heavily on the combustion of fossil fuels mainly due to their ease of handling, high energy density, and portability compared to many other forms of energy [1]. Yet, burning these fuels in internal combustion (IC) engines emits harmful pollutants like nitric oxides (NO_x) and soot, detrimental to human health, alongside carbon dioxide (CO_2), a significant greenhouse gas contributing to global warming [2], [3]. Hence, the need for cleaner and more efficient combustion processes and engines is imperative. Electric motors have yet to reach the performance and reliability standards set by IC engines in almost every application. They also rely on potentially scarce materials and use electricity often generated from the same fossil fuels they seek to replace.

Recent advancements in low-emission engine technologies such as homogenous charge compression ignition (HCCI), premixed charge compression ignition (PCCI), and reactivity-controlled compression ignition (RCCI) could help meet this need [4], [5]. In such engines, autoignition through cool flames plays a crucial role in combustion, yet this process remains inadequately understood. Furthermore, the thermal efficiency of existing IC engines, around 38%, has the potential to rise to 60% with the development of future ultra-lean and low-temperature engines that leverage cool flames.

Developing chemical kinetic models is essential to improving combustion systems for better efficiency and reduced emissions. These models, through computational analysis, and varied condition simulations, provide analytical insights

into autoignition, heat release and low-temperature kinetics. The research in this work focuses on studying cool diffusion flames utilizing autoignition delay characteristics of *n*-heptane autoignition simulations.

Additionally, enhancing our understanding of CDFs can significantly boost both fire safety and process safety measures. Typically, large-scale explosions are triggered by strong ignition sources, including electric arcs or open flames. However, a lesser-known ignition pathway involves weak ignition sources coupled with cool flames. For instance, it's suspected that the combination of air ingress and a cool flame was behind a notable industrial explosion [6]. Furthermore, the potential for CDFs to ignite and sustain themselves in the unique environment of spacecraft highlights their importance. The phenomena of smoldering fires transitioning into flaming ones are marked by conditions—specifically, gas temperatures and mixture ratios—that are favorable for CDFs. Additionally, spontaneous combustion incidents, such as those involving oily rags or biomass, occur at temperatures where CDFs are known to be stable.

1.1 A historical overview of Internal Combustion (IC) engines

The earliest evidence of a functioning engine dates back to the early seventeenth century, when Dutch mathematician and physicist Christiaan Huygens conducted experiments with gunpowder engines. Progressing from Huygen's initial experiments, the first commercial internal combustion (IC) engine was engineered by J.J.E. Lenoir in 1860. This model, a spark ignition (SI) engine, with a two-stroke cycle, was capable of delivering up to 6 hp and an efficiency of 5%. In 1867, German engineer N. A. Otto introduced an atmospheric engine that operated on a two-stroke cycle and achieved an

11% efficiency. By 1876, Otto had improved his design to incorporate a four-stroke cycle, substantially lightening the engine and boosting its efficiency to 14%. This development, together with a French patent granted in 1884, provided the essential groundwork for the IC engines of today, setting the standards for peak performance and efficiency [7], [8]. Despite numerous advancements aimed at reducing weight and enhancing power and efficiency, this engine type remains akin to those that drive the world today.

In 1892, R. Diesel, a German engineer obtained a patent for the diesel engine, a design that stood out because it operated under significantly higher pressure, enabling fuel to ignite on its own without the need for an external ignition source. Known as compression ignition (CI) engines, these engines have higher compression and expansion ratios, making them more efficient than spark ignition (SI) engines [8], [9]. Despite their efficiency, early diesel engines were criticized for being noisier, larger, and more polluting than their gasoline counterparts, which hindered their widespread adoption. While modern diesel engines have addressed many of these issues, they have not yet achieved the same prevalence as gasoline-powered SI engines.

These engines are fueled by products derived from crude oil; a non-renewable resource extracted from beneath the Earth's surface. SI engines commonly use gasoline, a highly volatile liquid consisting of various midsized hydrocarbons. Conversely, CI engines typically utilize diesel fuel, which is less volatile than gasoline and possesses a higher energy density.

1.2 Challenges associated with conventional IC engine technologies

The reliance on crude oil presents a significant challenge due to its finite supply. Currently, 70% of the daily global consumption of 86 million barrels of crude oil powers only IC engines. In the U.S. alone, 10 million barrels of crude oil is used every day in cars, plus 4 million in heavy duty vehicles [2]. Addressing the challenge of crude oil dependency necessitates the innovation of efficient engines and alternate powering methods for IC engines. This approach could significantly extend the lifespan of global oil reserves. Moreover, the exploration of alternative fuels like natural gas, alcohols, hydrogen, and synthetic fuels presents viable solutions for a sustainable future.

Hence, as society remains dependent on IC engines for transportation, commerce, and power generation, their economical and efficient usage is primarily obstructed by three key technological challenges: engine knocking, low thermal efficiency, and pollutant emissions.

Higher compression and expansion ratios are essential for improved engine designs. However, a major problem with higher compression ratios is that they lead to knocking. Engine knocking, also known as knock, is characterized by the uncontrolled and premature autoignition of the fuel-air mixture within the engine. Persistent knocking can lead to a decline in engine performance, damage to engine parts, and the emission of a loud, sharp noise. Knock is controlled by low temperature chemistry. A key indicator of a fuel's ability to prevent knock is its octane rating, which measures the autoignition resistance of the fuel-air mixture. The higher the octane rating, the greater is the fuel's capacity to resist knock, ensuring better combustion within an

engine. Initially, to boost the octane rating of gasoline, tetraethyl lead was added to the fuel. Although this technique was successful, it resulted in increased atmospheric lead particulates, posing serious health risks. Consequently, the use of lead in gasoline was prohibited globally. Nowadays, the octane rating of gasoline is enhanced through the process of catalytic reforming, bypassing the health hazards associated with lead [2], [10], [11], [12].

The thermal efficiency of an engine measures the ratio of energy utilized for work to the total energy generated through combustion. Unused energy is lost as heat into the surroundings. This efficiency is governed by the Carnot cycle, constrained by the engine's maximum and minimum operating temperatures. The maximum temperature an engine can withstand is determined by the properties of the engine materials and the auto-ignition characteristics of the fuel. Exceeding this temperature can lead to material degradation and increase the likelihood of engine knock. Modern diesel engines achieve 20-40% higher efficiency compared to SI engines. The net thermal efficiency for the majority of commercial vehicles currently in operation is around 40%. Figure 1.1 presents the schematic of input, output, and energy losses in an advanced diesel engine. It is evident that a considerable portion of the engine's thermal efficiency is diminished due to heat losses, which occur from the high-temperature flames to the engine walls and through the exhaust gas [9], [13].

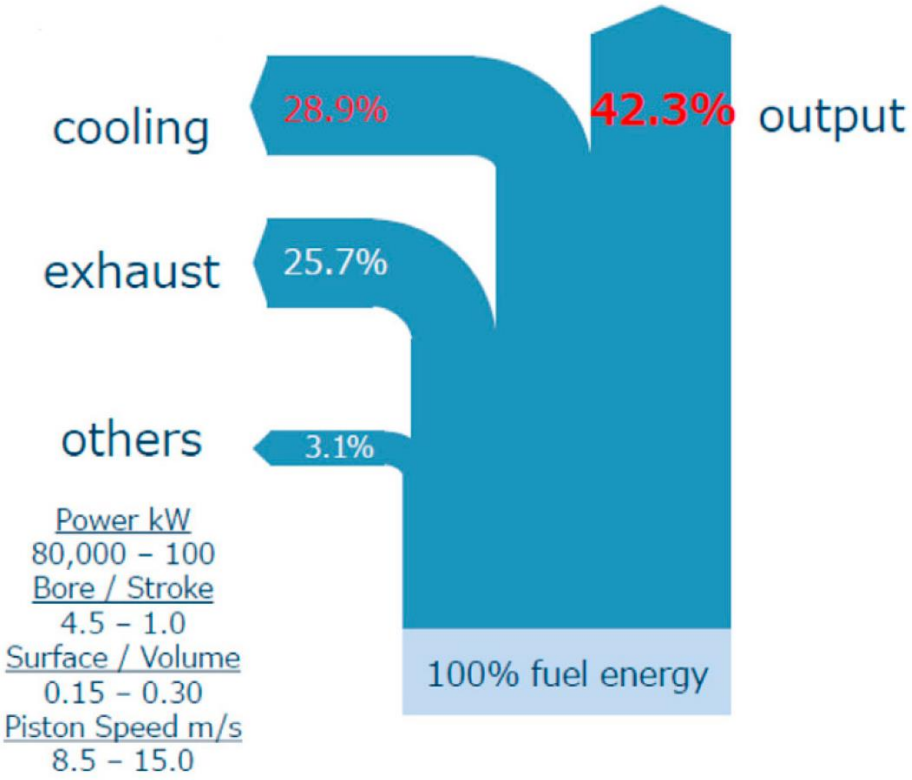

Figure 1.1. Schematic of heat balance of an automotive diesel engine

Reproduced from [13]

Apart from enhancing efficiency, the reduction of pollutant emissions stands as another primary motivator for ongoing research into IC engines. Significant pollutants include hydrocarbons (HC), carbon monoxide (CO), nitrogen oxides (NO_x), and particulate matter (PM). HC emissions result from incomplete combustion, producing irritants and potential carcinogens that contribute to smog. CO, a toxic gas, is emitted under high fuel-air ratios, lacking sufficient oxygen for complete combustion to CO_2. NO_x emissions, precursors to smog and surface-level ozone, arise at high temperatures and are linked to both SI and CI engines. Particulate matter, or soot, generated primarily in CI engines, poses risk to cardiovascular health [8], [14].

Addressing these emissions has led to legislative measures and the development of new engine technologies aimed at pollution reduction. Adjusting the fuel-air ratio can mitigate some emissions but may exacerbate others, illustrating the complexity of achieving optimal engine performance without environmental detriment. Innovations like thermal and catalytic converters have made strides in converting harmful pollutants to less harmful forms, though challenges remain, particularly during engine startup. Ongoing efforts in the automotive industry aim to design engines that inherently produce fewer pollutants through strategies such as fuel dilution and leveraging cool flame chemistry for lower temperature operations, underscoring a continued commitment to both efficiency and environmental responsibility in IC engine development.

1.3 Background and history of cool flame studies

Premixed cool flames were first observed by Davy in the early 19th century [15]. Initially considered a novelty, subsequent observations of the flame were driven by scientific curiosity, with efforts aimed at characterizing the phenomenon and integrating it into the existing understanding of combustion processes. Research during the 1920s and 1930s focused predominantly on the study of premixed cool flames generated by alkanes, ethers, and aldehydes in flow tubes and flow reactors. Over the time since, the significance of cool flames has increased markedly, especially after their role in causing engine knocking was identified [16].

It was only in the past decade that the existence and observation of cool diffusion flames was first discovered in *n*-heptane droplet experiments aboard the International Space Station (ISS) [17], [18]. Unlike cool premixed flames that

propagate into a premixture, cool diffusion flames receive fuel and oxidizer from opposite sides, with the components reaching the flame through diffusion. A thorough investigation of both premixed and diffusion cool flames is essential for a comprehensive understanding of cool flame chemistry, given the significant differences in equivalence ratios and temperature distributions between these two types of flames.

Observationally, a cool flame is characterized by a faint blue luminescent reaction front, setting it apart from hot flames through several distinct characteristics: they exhibit peak temperatures ranging from 500 to 1000 K [19], induce a modest increase in gas temperature by 2 to 200 K [20], consume a small fraction of the reactants and produce a substantial amount of formaldehyde [13], [15], [21].

Historically, the study of cool flames has predominantly taken place in controlled laboratory settings, utilizing autoignition phenomenon in rapid compression machines (RCMs) and low-temperature shock tube experiments. In these setups, the reactive mixture is quickly compressed to temperatures and pressures that mimic the conditions found in engines where cool flames are observed. Following an initial delay, a cool flame warms the mixture until a subsequent temperature rise self-extinguishes it. This may be followed by a longer delay and then a rapid transition to full, high-temperature ignition. This progression from cool to hot ignition, termed "two-stage" ignition, sees the cool flame's heat accelerate final ignition, effectively "sensitizing" the mixture by raising temperatures while using minimal fuel. Figure 1.2 shows a representative two-stage ignition process for a high pressure (13.5 bar) mixture of *n*-heptane in air, where the temperature of the mixture relative to its final value of 750 K is plotted as a function of time [22].

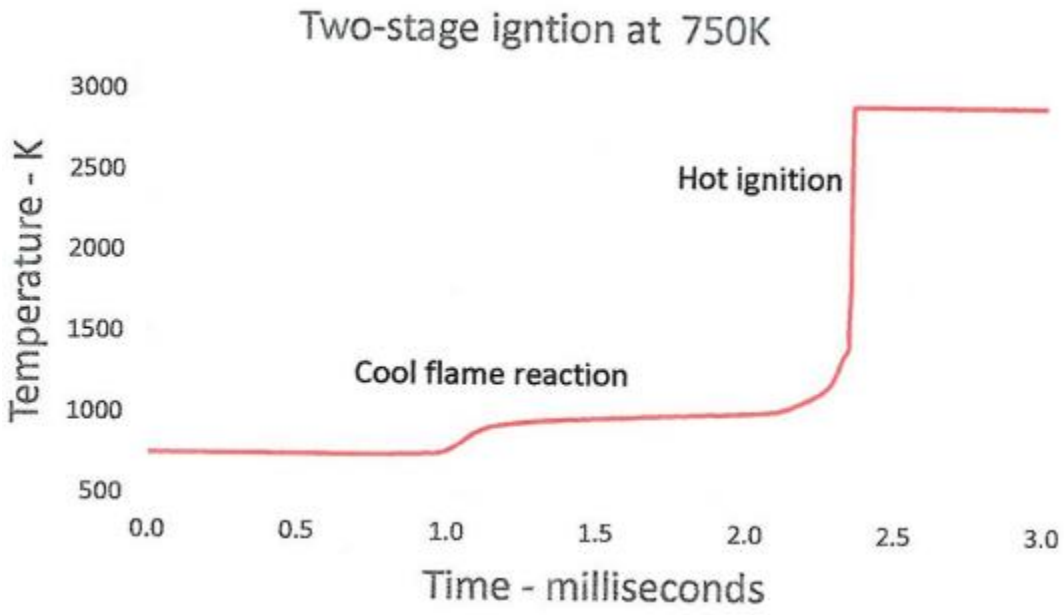

Figure 1.2. Temperature versus time history for a *n*-heptane/air mixture at 13.5 bar

Reproduced from [22]

Cool flames only exist within the Negative Temperature Coefficient (NTC) regime [23]. The NTC region is a unique phenomenon, in which the overall reaction rate decreases with increasing temperature [24], [25]. Within the NTC regions, an increase in the peak temperature causes deceleration of the chemistry. Consequently, as the rate of heat release diminishes, there is a corresponding drop in the peak temperature. Conversely, a reduction in temperature prompts the chemical reactions to enhance the rate of heat release, leading to a rise in temperature towards a stable level. These Negative Temperature Coefficients (NTCs) are observed around the crossover temperature, where alkyl radicals are depleted at equivalent rates by both cool and hot flame chemical processes.

1.4 The role of low-temperature combustion in advanced engines

In the realm of low-emission technologies, innovations like Homogenous Charge Compression Ignition (HCCI), Premixed Charge Compression Ignition (PCCI), and Reactivity Controlled Compression Ignition (RCCI) have attracted considerable interest. HCCI engines mimic Spark Ignition (SI) engines by introducing a pre-mixed blend of fuel and air into the combustion chamber, while PCCI engines draw inspiration from Compression Ignition (CI) engines in their approach to fuel injection. RCCI engines distinguish themselves by employing fuels of different reactivities, optimizing the combustion process across both low and high temperature regimes. The autoignition process of cool flames is a critical aspect of the combustion process in these engines, significantly influencing their efficiency and emission profiles [2], [5], [26], [27].

LTC engines share basic operating principles with SI and CI engines, utilizing the thermal energy from combustion to generate mechanical power. As a subclass of CI engines, LTC engines ignite fuel without an external spark, relying instead on compressing the fuel-air mixture until it auto-ignites. The distinctive feature of LTC technology is its reliance on cool flame autoignition rather than traditional hot flame ignition, made possible by extremely lean fuel-air mixtures. In LTC engines, ignition happens simultaneously at various points within the mixture, leading to a quicker pressure rise compared to traditional CI engines, but with a significantly reduced temperature increase. Hence, LTC engines use high compression ratios to their advantage and lose less heat to the combustion chamber walls because the temperature difference is smaller [2], [4], [28], [29].

The rapid movement of the cool flames shorten the ignition time, crucial for operating an engine with substantial flue gas recirculation. Moreover, these cool flames accelerate the formation of ignition kernels – tiny, localized sites of high temperature that support a fully burning flame in fuel-lean regions.

LTC engines also see a decrease in certain harmful emissions commonly found in internal combustion (IC) engines, notably NO_x and particulate matter (PM). The creation of these pollutants is linked to high temperatures, well above the cool flame peak temperatures of around 1000 K, resulting in significantly lower levels of these emissions in the exhaust of LTC engines. Research has demonstrated that LTC engines can cut NO_x emissions by up to a thousand times and reduce soot emissions by six times compared to traditional diesel engines, all while achieving a 16% increase in efficiency [28]. Additionally, these engines are versatile in terms of fuel usage; theoretically, any fuel capable of supporting cool flame combustion could be utilized.

The advancement of LTC engines comes with its own set of challenges. Unlike SI and CI engines, the ignition timing in LTC engines is not as easily controlled, making it hard for these engines to operate efficiently across a broad spectrum of conditions. Specifically, at high loads, engines like HCCI and PCCI tend to produce excessive noise and experience knocking. RCCI engines are being developed to address this issue by blending the advantages of both low and high temperature combustion, thereby enhancing efficiency across various operating conditions. However, the lower heat release associated with LTC leads to diminished power output, which restricts the application of this technology to less demanding uses. Additionally, the cool flame process results in lower consumption of reactants, leading to higher emissions of HC

and CO in LTC engines compared to their SI and CI counterparts. This is because at the cooler temperatures, hydrocarbons that get trapped in nooks or stick to the combustion chamber walls fail to burn, and CO is not fully converted into CO_2. LTC engines are also known to emit significant amounts of certain compounds that are not typically released by CI and SI engines, notably formaldehyde—a substance with known irritant and carcinogenic properties that can also contribute to the formation of ground-level ozone. Polycyclic aromatic hydrocarbons, recognized for their carcinogenic risks, are another concern [29]. Tackling these issues necessitates a deeper insight into the cool flame chemistry that drives LTC engines. Such knowledge would enable the creation of detailed models to evaluate engine performance under diverse conditions.

1.5 Cool flame oxidation kinetics

The oxidation process of hydrocarbons with air or oxygen involves a multifaceted series of reactions rather than a straightforward, one-step oxidation to yield carbon dioxide and water as the ultimate outcomes. In practice, the mechanism of the process involves many intermediate compounds, like carbon monoxide, aldehydes, ketones, alkenes, and oxygenated species [30]. A general oxidation reaction can be divided into three mechanisms, namely: initiation, propagation, and termination.

In the initiation stage, fuel is converted into radicals:

$$RH \rightarrow R^{\bullet} + H^{\bullet} \quad (1.1)$$

Or

$$RH + O_2 \rightarrow R^{\bullet} + HO_2 \quad (1.2)$$

Where RH denotes any hydrocarbon and $R^{\bullet}$ is its radical. At low temperatures, formation of the HO_2 radical is favored. However, at low temperatures, the rate of

reaction for Eq. 1.2 is much less than for Eq. 1.1, so the initiating oxidation reactions occur mainly through reaction 1.1. Additionally to Eq. 1.1 and 1.2, especially higher alkanes (C4 or higher) may also decompose thermally forming two alkyl radicals. Following the initial oxidation reaction, which involves only the compounds originally present in the mixture, a series of secondary oxidation reactions occur where the newly formed compounds interact among themselves and with the remaining unburned fuel.

$$RH + X \rightarrow R^{\bullet} + \acute{X} \tag{1.3}$$

Where X represents, depending on the conditions, $H^{\bullet}$, $^{\bullet}OH$, $O^{\bullet}$ and $HO_2^{\bullet}$ radicals forming H_2, H_2O, $^{\bullet}OH$ and H_2O_2, respectively.

When initially radicals are formed, they react with other compounds present in the mixture (propagation) by a straight chain or a chain branching mechanism. When the rate of radical formation is lower than the rate of radical termination of newly formed radical, the termination stages begins, and the oxidation reaction ceases. Hence, the oxidation proceeds through many intermediate compounds, whose formation is more pronounced at low temperatures, including aldehydes, ketones, alcohols, alkenes, peroxides, and carbon monoxide. It can be broadly asserted that the oxidation chemistry of hydrocarbons is influenced by the system's temperature, pressure, and oxygen concentration. The oxidation path with respect to temperature can be divided into:

- A low temperature regime, where peroxy oxidation chemistry occurs.
- An intermediate temperature regime, where HO_2 and H_2O_2 chemistry dominates.
- A high temperature regime, where small size radical chemistry occurs.

In the low temperature regime, a hydrogen atom is removed from a hydrocarbon molecule to form an alkyl radical (R). This alkyl radical reacts with an oxygen molecule

forming a peroxy radical (RO_2) which further isomerizes to form QOOH (Q = C_nH_{2n}) radical.

$$R + O_2 + M \rightarrow RO_2 + M \quad (1.4)$$

$$RO_2 \rightarrow QOOH \quad (1.5)$$

QOOH can decompose to form an olefin and HO_2 molecule, or a cyclic ether and OH molecule.

$$QOOH = QO + OH \quad (1.6)$$

$$QOOH = Q + HO_2 \quad (1.7)$$

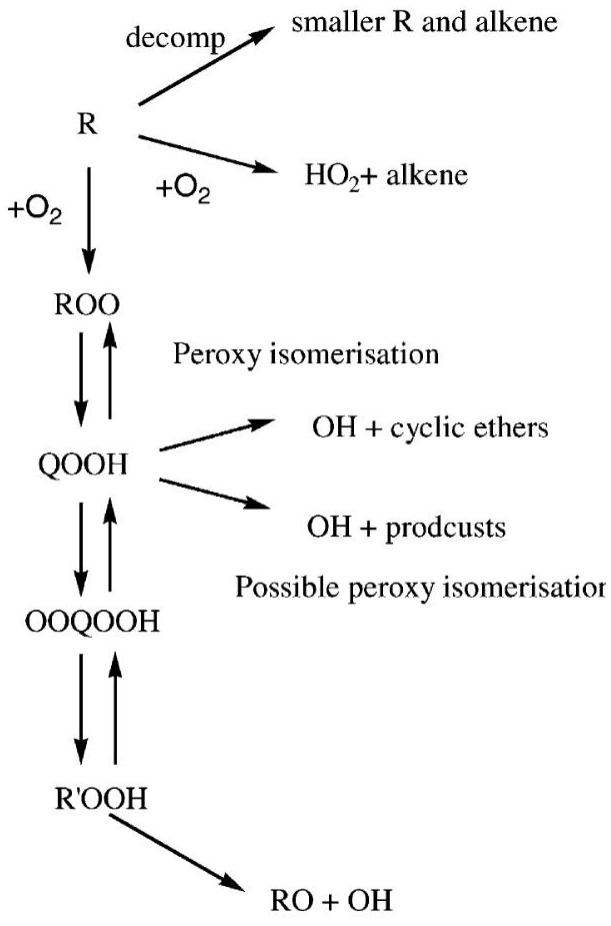

Figure 1.3. Simplified alkane low temperature oxidation mechanism

Reproduced from [30]

QOOH also has a chance to attach with another O_2 molecule and form Q_2QOOH. This molecule breaks down into a ketohydroperoxide and OH molecule.

$$QOOH + O_2 = O_2QOOH \quad (1.8)$$

Ketohydroperoxide decomposes at around 800 K and therefore, the low temperature oxidation path ceases at high temperatures. This temperature is also lower than the H2O2 decomposition range. Figure 1.3 shows a schematic of hydrocarbon oxidation process similar to the process explained above.

In the intermediate temperature range of 850 – 1200 K, OH formation to sustain chain branching is dependent on the following reactions:

$$H + O_2 + M = HO_2 + M \quad (1.9)$$

$$RH + HO_2 = R + H_2O_2 \quad (1.10)$$

$$H_2O_2 + M = OH + OH + M \quad (1.11)$$

Finally, at temperatures above 1200 K, Equation 1.12 takes over reaction 1.9 and becomes the most important reaction controlling combustion rate.

$$H + O_2 = O + OH \quad (1.12)$$

The final stage in the high temperature regime is the oxidation of CO by OH radical with release of CO_2 and H_2O.

$$CO + OH = CO_2 + H_2O \quad (1.13)$$

The H atom required to start this reaction is released from thermal decomposition of alkyl radicals, which is possible at only higher temperatures.

1.6 Motivation and Objective

To broaden our understanding and address the existing gaps regarding cool flames and the associated phenomenon, it is vital to involve researchers from diverse

disciplines in this field of study. However, the majority of studies on cool diffusion flames (CDF) utilize equipment and resources beyond the reach of a typical researcher. Therefore, developing chemical kinetic models that aid in predicting the behavior of cool flames, two-stage ignition and practical combustion systems becomes imperative.

These models offer crucial analytical insights by bridging the gap between experimental findings and theoretical frameworks. A distinctive aspect of these zero-dimensional kinetic models is their function as a 'thought experiment,' allowing researchers to explore hypothetical scenarios with the question 'What if...?' even if those specific conditions or changes cannot be directly tested through experiments. Therefore, as previously discussed, grasping the autoignition process is crucial for a comprehensive understanding of phenomena such as cool flame behavior, two-stage ignition, and low-temperature heat release. The autoignition delay is a vital parameter for evaluating the efficacy of kinetic models, as it is frequently used to validate the precision of combustion chemistry models [31].

Furthermore, the significance of cool flames extends beyond engine research and development to include areas like fire safety, where scenarios involving hydrocarbon vapor and air mixtures encountering hot surfaces or remaining in heated chambers are studied. Studies have also explored the initiation of fires in aircraft fuel tanks through both low-temperature and two-stage ignition processes, focusing on the shift from cool to hot flame ignition. This research is vital for preventing fires and explosions in aircraft fuel tanks, as they are subject to high temperatures and low pressures at high altitudes, leading to potential ignition via cool flame, hot flame, and two-stage ignition chemistries [32], [33]. Additionally, the investigation into the 1996

Flight TWA explosion, which resulted in the loss of over 200 lives, highlighted that a cool flame ignition could be a contributing factor [34]. The ability of cool flames to occur beyond the conventional flammability limits of hot flames highlights the importance of this research in enhancing fire safety.

Thus motivated, the objective of this study is to understand the autoignition behavior of *n*-heptane at varied temperatures and equivalence ratios using chemical kinetic mechanisms. A key focus is on gaining insights about cool diffusion flames using autoignition simulations and the ability of these mechanisms to accurately predict phenomena associated with them, such as the two-stage ignition process and the effect of varied initial mixture temperatures on ignition delay times. A wide variety of chemical kinetic mechanisms available in the literature are also studied to establish a threshold for the Negative Temperature Coefficient (NTC) regime.

Chapter 2: Research and Methodology

2.1 The use of autoignition simulations in premixed and non-premixed combustion and the associated delay time

Combustion processes can typically be divided into two primary categories: premixed and non-premixed combustion, with a range of partial mixing levels of the fuel and oxidizer taking place across the spectrum between these two types. Ignition of both premixed and non-premixed fuels can happen via spark ignition (SI) or through the process of compression ignition (CI), which is often termed autoignition.

Autoignition significantly differentiates diesel engines (CI engines) from gasoline engines (SI engines). Autoignition refers to the self-ignition of a homogenous mixture of fuel and air. In premixed combustion systems, like those in SI engines, spark ignition is initiated by applying a specific amount of heat or energy, which forms an ignition kernel that expands and sustains itself. For these engines controlling autoignition is paramount. If uncontrolled, this process can result in 'knocking' due to the spontaneous combustion of part of the end-gas. Thus, understanding the conditions and temperature that induce autoignition is crucial to avert damage and increase operational efficiency.

In contrast, autoignition is central to the combustion process in CI engines, profoundly impacting their performance, fuel efficiency, and emission levels. The operating principle of these engines involves generating an air-fuel mixture that auto ignites under conditions of elevated temperature and pressure without the need of an external spark [8].

The occurrence of autoignition is influenced by several factors, including the mixture's initial temperature, chemical composition, and pressure, as well as, in the case of turbulent flows, the levels of local turbulence and composition gradients. The ignition timing (or the autoignition delay time) and the pathways for chain branching are primarily determined by whether the initial temperature exceeds the autoignition temperature (AIT) of the given fuel. Moreover, as explained in the earlier sections, autoignition of cool flames plays an integral part in combustion process in advanced engine technologies.

Extensive evidence shows that the chemical reactions leading to the ignition of a fuel-air mixture necessitate a specific duration [35]. This period, commonly known as the ignition delay time (IDT), is an important physiochemical property of combustible fuel-air mixture in engine operations. Typically, IDTs are determined through experimental methods, providing a foundational basis for enhancing engine design and optimizing combustion processes [36].

The instant of ignition is characterized by the formation of a large quantity of hydroxyl radical, atomic oxygen, hydrogen, and molecular combustion products. A long ignition delay time may lead to steep pressure rise and failure of the combustion chamber and to 'rough' running of the engine accompanied by knocking. Similarly, a short ignition delay time may lead to incomplete combustion of the fuel and, consequently, to smoke formation, power loss, and reduced efficiency of the engine. Hence, a major requirement for smooth start and steady running of jet engines and soft running of diesel engines under different conditions is constant ignition delay with respect to mixture composition at a fairly short absolute delay time [37].

Measured IDTs are much used parameters against which numerical models are tested. They may be derived in a wide range of experimental systems for various fuels and thus constitute a useful route to testing a model over extensive range of conditions. The main experimental sources used to derive IDTs are closed vessels, rapid compression machines, shock tubes and certain types of tubular flow systems [38].

Therefore, accurately predicting autoignition, by accounting for both ignition temperature and ignition delay time under varied conditions, is vital for providing insights into the Negative Temperature Coefficient (NTC) behavior, the two-stage ignition process, cool flame phenomena, and the dynamics of low-temperature kinetics. Understanding these aspects can lead to improved management of engine performance.

2.2 Simulation methodology

The cetane number (CN) refers to the ignition quality of the fuel. The higher the CN, the lower is the ignition delay time. Traditional diesel fuel is a complex mixture of various hydrocarbons (HCs), distinguished by a high cetane number. Among these, *n*-heptane is particularly significant, not only because it serves as a primary reference fuel (PRF) for the octane rating in internal combustion (IC) engines but also due to its CN, which is comparable to that of diesel and its high carbon content [39]. Hence, *n*-heptane is frequently utilized as an alternative to diesel in both experimental and computational research. Investigating the autoignition characteristics of *n*-heptane can provide critical insights into phenomena such as ignition delay time, two-stage ignition, and cool flames. This alignment of attributes establishes *n*-heptane as the optimal choice for our study [40].

Simulations of autoignition were performed utilizing the Cantera code, an open-source software for chemical kinetics simulation. Cantera enables time-efficient investigation of existing and potential new processes as compared to direct laboratory investigations. It finds application in a variety of fields such as combustion, detonations, electrochemical energy conversion and storage, fuel cells, batteries, aqueous electrolyte solutions, plasmas, and thin film deposition. The software streamlines the process of incorporating detailed chemical thermo-kinetics, and transport models into calculations by the automating the chemical kinetic, thermodynamic and transport computations, allowing users to conduct comprehensive analyses with efficiency [41].

It facilitates simulations in a Cantera Reactor that represents the simplest form of a chemical reacting system. It corresponds to an extensive thermodynamic volume V, in which all state variables are homogenously distributed. The system is generally unsteady - that is, all states are functions of time. In particular, transient state changes due to chemical reactions are possible. However, thermodynamic (but not chemical) equilibrium is assumed to be present throughout the reactor at all instants of time [42]. Although the program offers a range of reactor options, for this study we specifically utilized the Ideal Gas Constant Pressure Reactor. This is a homogeneous, constant pressure, zero-dimensional reactor for ideal gas mixtures. The volume of the reactor changes as a function of time in order to keep the pressure constant. The choice of this reactor for our study was particularly driven by its inherent simplicity and the advantage of reduced run times. Temperature and pressure of the initial mixture are assigned as inputs before the start of the simulation. Additionally, it allows for the

customization of the gas mixture within the reactor, including setting the equivalence ratio, selecting the fuel species, and determining the oxidizer composition. The program exports the state of the "gas" over time, and records the changes in the gas composition, temperature, etc. as the simulation progresses. The Cantera program requires a chemical kinetics mechanism file as an input.

2.3 Chemical kinetic mechanism

A chemical kinetic mechanism is comprised of species that have specific thermodynamic and transport properties, along with elementary chemical reactions and their corresponding rate constants. These mechanisms can vary greatly in complexity, ranging from a single reaction to many thousands, depending on the specific needs and computational resources available. For instance, the conversion of hydrogen to water through oxidation is more complex than can be captured by a simple global reaction equation. Hydrogen requires eight species and approximately 30 elementary reactions to describe its oxidation over a wide range of pressure and temperature [43].

An elementary reaction specifies the reactant and product species and the associated rate constant. By understanding the forward rate constant and the thermochemical characteristics of the reacting species, one can compute the reverse rate constant, ensuring consideration for thermodynamic equilibrium. Hence, a chemical kinetic model contains a list of both the species with their thermodynamic parameters and all of the elementary reactions and their associated accurate rate constants and third body collision efficiencies that account for variations in temperature and pressure [43].

In comprehensive chemical kinetic schemes, all conceivable reactions involving the fuel and its intermediates are included. For a mechanism to be considered thoroughly comprehensive, it should not only be accurate for a specific fuel but also for its smaller constituent fuels [44].

This chemical kinetic mechanism has been provided as an input to Cantera, a numerical model that simulates a practical reactor. Cantera solves a series of differential equations that requires initial conditions from the experiments to be simulated. The integration of these equations proceeds in timesteps using integration control to ensure that the species, temperature, and pressure do not change considerably in any one timestep so that the overall calculations are accurate.

Developing a chemical kinetic mechanism involves a dual approach. Initially, it requires collecting kinetic data from targeted experimental and computational studies. These studies provide details on reaction rate coefficients and their dependencies on temperature and pressure, as well as information on branching into different products. Subsequently, these kinetic mechanisms are tested and validated against laboratory data that reflect macroscopic properties. The most critical of these properties include ignition delay time, flame propagation, and extinction strain rate.

However, complete knowledge of every reaction is not available, and since all known reaction rate parameters carry some degree of uncertainty, it is extremely difficult to attain a truly complete mechanism. Tools such as sensitivity and reaction path analyses are often employed to identify important reactions and intermediate species at different operating conditions, including temperature, pressure, and concentration [45].

2.4 N-heptane kinetic mechanisms with cool flame chemistry

The CRECK modeling group, based at Politecnico di Milano, specializes in the development of detailed kinetic models for diverse materials, serving as a valuable resource for the design and numerical analysis of combustion processes and industrial engines.

A major part of this research focuses on the *n*-heptane high plus low temperature (HT+LT) mechanism version 2003, March 2020, provided by CRECK, featuring 339 species and 9781 reactions [46]. This mechanism was chosen because it is able to resolve both high and low-temperature kinetic regimes, which is necessary for studying and simulating the two-stage ignition process, the Negative Temperature Coefficient (NTC) regime and the occurrence of cool flames.

In Section 3.5, several other kinetic mechanisms available in the literature have also been evaluated, namely the n-heptane detailed mechanism version 3 by Lawrence Livermore National Laboratories (LLNL) [47], the n-heptane mechanism by National University of Ireland Galway (NUIG) [48], the complete San Diego mechanism with heptane chemistry provided by the University of California San Diego (UCSD) [49], the n-heptane mechanism by California Institute of Technology (CALTECH) [50], and the Jerzembeck detailed mechanism provided by the European Center for Research and Advanced Training in Scientific Computing (CERFACS) [51].

Chapter 3: Results and Discussion

3.1 Temperature versus time behavior

The previously outlined CRECK mechanism has been utilized to compute a temperature versus time history for a stoichiometric gas mixture of *n*-heptane/air at atmospheric pressure (101325 Pa), with initial mixture temperatures of 450 – 1000 K. The model predicts the temperature and species concentrations at discrete time steps.

Figure 3.1 shows a sample temperature versus time trajectory for such a mixture at an initial temperature of 650 K. A distinct two-stage ignition process can be seen. The mixture begins to heat up from 650 K, experiencing only a slight temperature increase. The first stage of ignition is observed at 0.08 s, when the temperature reaches 760 K, which causes a rise in the initial mixture temperature of 110 K. Subsequently, the temperature rises steadily again until it approaches 950 K. At this point, a rapid increase in temperature is observed, indicating the second stage of ignition at 0.46 s and at a temperature of 1710 K. The temperature of the mixture continues to rise until it reaches its final temperature of 2400 K, which corresponds to the adiabatic flame temperature of the mixture.

A sample trajectory at a higher initial mixture temperature of 750 K is shown in Figure 3.2. Interestingly, the time taken to reach the first-stage ignition is reduced by about five times, down to 0.017 s, while maintaining the ignition temperature at 760 K. In contrast to the decrease in time for the first-stage ignition, the time for the second-stage ignition notably increased to 1.19 s, rather than decreasing. The second-stage ignition temperature also increased to 1780 K.

Figure 3.3 shows another sample trajectory, this time for a mixture with an initial temperature of 850 K. This trajectory is markedly distinct from those at the other two mixture temperatures of 650 and 750 K, as it exhibits only a single-stage ignition process. The ignition for this trajectory occurs at 0.67 s and at a temperature of 1810 K.

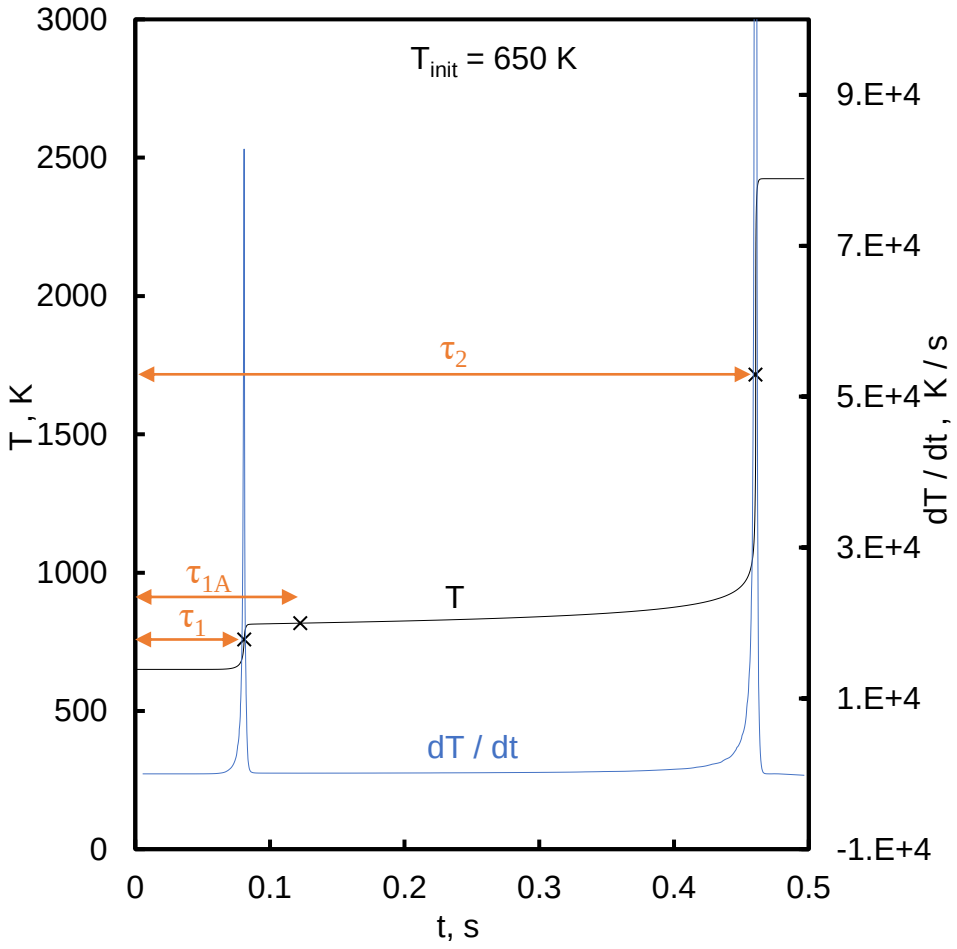

Figure 3.1. Temperature versus time history for *n*-heptane/air mixture at atmospheric pressure and initial mixture temperature of 650 K. This is an example of a two-stage ignition process

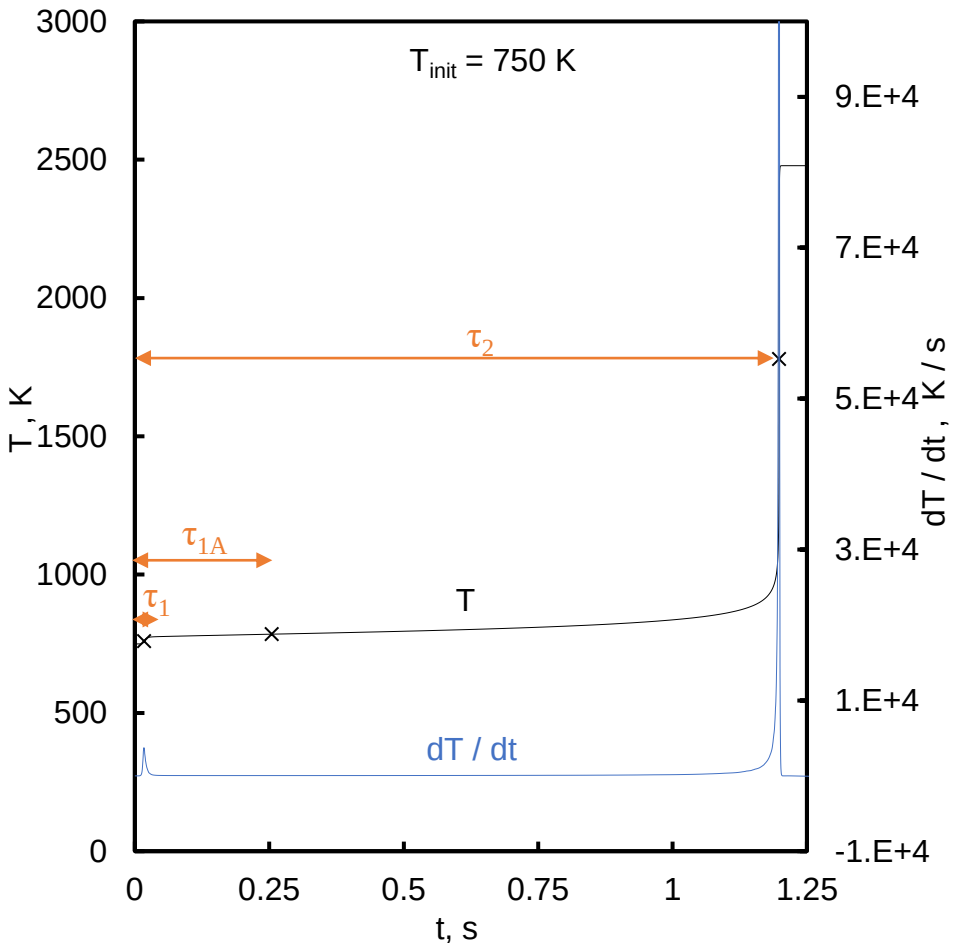

Figure 3.2. Temperature versus time history for *n*-heptane/air mixture at atmospheric pressure and initial mixture temperature of 750 K. This is an example of a two-stage ignition process

The observation of two-stage ignition process is particularly prominent for initial mixture temperatures up to 775 K. Above this temperature, only a single-stage ignition process is typically seen. The first-stage ignition process is driven by low temperature chain-branching peroxy chemistry. After first-stage ignition, the temperature rises slowly via oxidation of the intermediate species by O_2, OH, and HO_2. As the temperature further increases to a critical temperature, second-stage ignition occurs, which results in a significant temperature rise. The oxidation process at this

stage is governed by high-temperature chain branching reactions. Since these high-temperature chain branching reactions do not have ceiling temperature, the temperature rise continues until the time when almost all the fuel and intermediate species are oxidized resulting in formation of H_2O and CO_2.

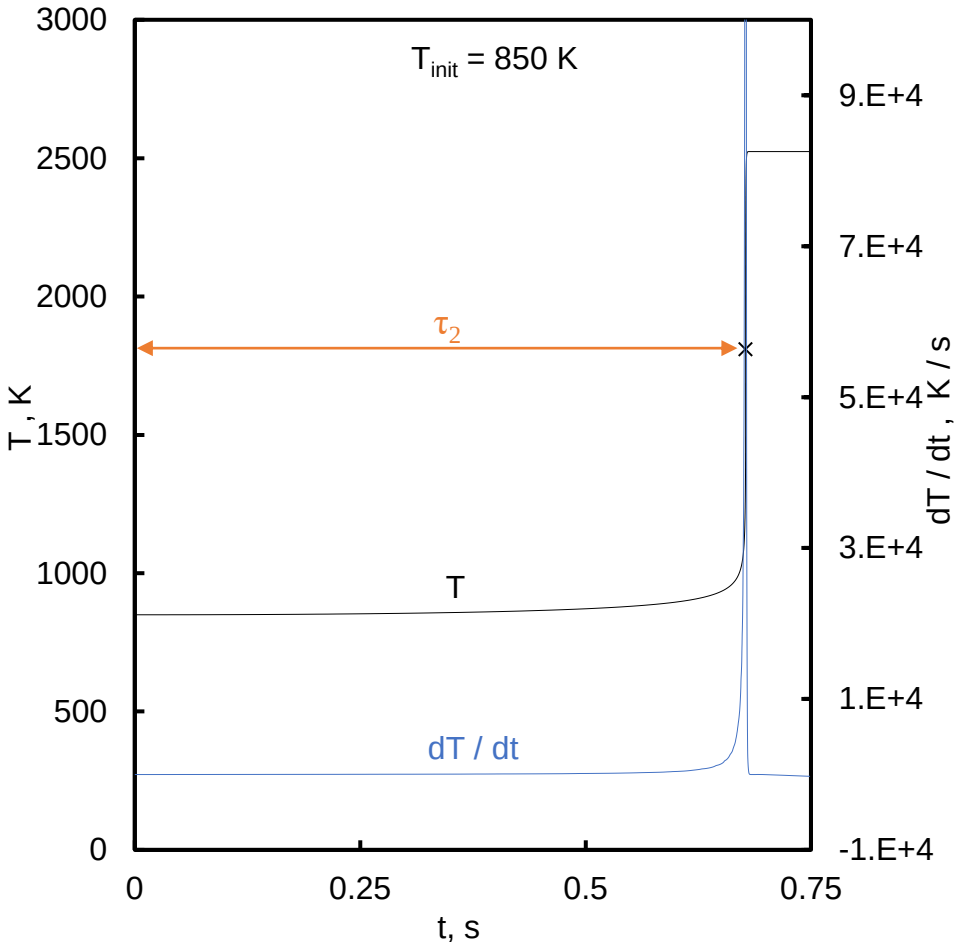

Figure 3.3. Temperature versus time history for *n*-heptane/air mixture at atmospheric pressure and initial mixture temperature of about 850 K. This is a single- stage ignition process

The estimation of the rate of temperature increase (dT/dt) at a discrete time step was investigated. Initially, a rudimentary two-point approximation technique was employed, encompassing three sequential data points – specifically (t_{i-1}, T_{i-1}), (t_i, T_i),

and (t_{i+1}, T_{i+1}) as illustrated in Eq. 3.1, where 't' denotes time and 'T' signifies the temperature.

$$\left(\frac{dT}{dt}\right)_i = \frac{T_{i+1} - T_{i-1}}{t_{i+1} - t_{i-1}} \tag{3.1}$$

This approach is excellent for temporal uniform spacing, however, autoignition simulations are generally non-uniform.

Subsequently, an advanced numerical differentiation technique was adopted, notably a three-point parabolic approximation as shown in Eq. 3.2. This technique fits a parabola through each set of three consecutive points and finds the derivative of the parabola at central point x_i.

$$\left(\frac{dT}{dt}\right)_i = 2A(t_i) + B \tag{3.2}$$

Where,

$$A = \frac{T_{i-1} - T_i}{t_{i-1}^2 - t_i^2} - \frac{T_i - T_{i+1}}{t_i^2 - t_{i+1}^2}$$

$$B = \frac{T_{i-1} - T_i - A(t_{i-1}^2 - t_i^2)}{t_{i-1} - t_i}$$

The trajectories of the computed rate of temperature increase (dT/dt) using the three-point parabolic approximation method corresponding to the temperature versus time histories are plotted in Figure 3.1 – 3.3 using a solid blue line. These trajectories have one or two well-defined peaks depending upon the type of ignition.

The first such peak represents the first-stage ignition process, also referred to as the LTI (low temperature ignition), or the cool flame. This is characterized by the moment when the rate of temperature increase reaches its first local maximum. The heating during this time arises from the thermal effects of low temperature chemistry (LTC) reactions. The period from the start of the simulation to the point where the first-

stage ignition occurs, specifically the first local maximum in the rate of temperature rise, is defined as the first-stage ignition delay time (τ_1). This is marked by an 'x' on the plots. For instance, in Figure 3.1 and Figure 3.2, the respective first-stage ignition delay times are 0.08 s and 0.017 s. Figure 3.3 does not represent a two-stage ignition process and therefore a first-stage ignition delay time is not observed.

The second peak represents the second-stage ignition process, also referred to as the HTI (high temperature ignition), or the hot flame. This is characterized by the moment when the rate of temperature increase reaches its second local maximum. The heating during this time arises from the thermal effects of high temperature chemistry (HTC) reactions. The period from the start of the simulation to the point where the second-stage ignition occurs, i.e., the second local maximum in the rate of temperature rise occurs, is defined as the second-stage ignition delay time (τ_2). This is also marked by an 'x' on the plots. For instance, in Fig. 3.1, 3.2, and 3.3, the respective second-stage ignition delay times are 0.46, 1.32, and 0.67 s.

First-stage and second-stage ignition typically occur in close proximity, with a relatively short time interval separating them. Therefore, pinpointing the conclusion of the first-stage ignition process or the termination of cool flame is essential. To determine the end of the first-stage ignition process, the strategy of locating the local minimum has been utilized. The period from the start of the simulation to the point where the first-stage ignition ends, i.e., the local minimum in the rate of temperature rise occurs, is defined as the end of the first-stage ignition (τ_{1A}). This is marked by an 'x' between the first-stage and total ignition delay times. For example, in Fig 3.1 and 3.2, the end of the first-stage ignition is marked at 0.12 and 0.25 s, respectively.

Initial mixture temperatures at 650, 750 and 850 K are examined in detail below with the view toward understanding cool flame behavior, two-stage ignition, and the effect of varying conditions on ignition delay times.

Figure 3.1 shows a representative two-stage ignition process of stoichiometric gas mixture of *n*-heptane/air under initial temperature of 650 K and atmospheric pressure (101325 Pa). It is evident that initially the mixture exhibits a slow reaction rate with negligible temperature increase. This phase persists until a first-stage ignition delay time (τ_1) of approximately 0.08 s, marking the onset of the first stage of ignition (LTI), or the cool flame, as indicated by the initial peak in the rate of temperature increase (dT/dt). This stage rapidly elevates the mixture temperature to around 820 K, which also represents the end of the cool flame phase at 0.12 s. Subsequently, the rate of reaction is again relatively slow, until the temperature approaches approximately 950 K. At this point, the rate of reaction increases sharply, as evidenced by the second peak in dT/dt, marking the onset of the second stage of ignition, or the hot flame, where all of the remaining fuel is burned as the flame rapidly ignites. In this scenario, the second-stage ignition delay time (τ_2) is about 0.46 s.

Figure 3.2 shows a representative two-stage ignition process of stoichiometric gas mixture of *n*-heptane/air under initial temperature of 750 K and atmospheric pressure (101325 Pa). It is interesting to note that the second-stage ignition delay time (τ_2) extends to approximately 1.2 s, contrary to the expectations of a decrease, although since the initial mixture temperature has increased to 750 K. The initial peak has also diminished. At this point, the first-stage ignition is hardly discernible, and the increase

in the increase in delay time is clearly equivalent to an increase in the second stage of ignition.

Figure 3.3 shows a representative single-stage ignition process of stoichiometric gas mixture of *n*-heptane/air under initial temperature of 850 K and atmospheric pressure (101325 Pa). The ignition process is now essentially single-stage with no clearly discernible first-stage ignition peak. Additionally, the second-stage ignition delay time (τ_2) has also decreased to about 0.70 s.

As shown in fig. 3.1. and 3.2, the temperature versus time profile exhibits a noticeably clear two-stage temperature increase with a considerably long $\tau_{2\text{-}1}$. However, further increasing the initial mixture temperature beyond 775 K results in a vanishment of delay time τ_1. The disappearance of τ_1 is not due to insufficient time stepping in the simulation, instead, it is due to the vanishment of the initial peak in the temperature increase rate. This concludes that there is no sudden heat release that would indicate a low temperature ignition or a cool flame. It is also interesting to note that as the initial temperature keeps increasing from 450 K to 1000 K, the peak heat release rate of the LTI keeps decreasing until it finally reaches a point where it finally disappears. As the initial mixture temperature is further increased beyond 775 K, the process is now mainly dominated by intermediate to high temperature reactions.

Therefore, as the initial mixture temperature becomes sufficiently high (e.g., 800 K at 1 atm), the LTI stage and the associated low-temperature reactivity disappear, and only single-stage HTI remains. Hence, the fuel oxidation chemistry and ignition processes are highly dependent on the initial mixture temperature.

Table 3.1 shows the calculated first-stage ignition, first-stage conclusion and second-stage ignition delay times and the corresponding ignition temperatures for initial mixture temperatures ranging from 450 – 1000 K. For initial mixture temperatures ranging from 800 – 1000 K, only single – stage ignition behavior is observed. Temperature versus time history for initial mixture temperatures that have not been discussed above are included in Appendix B.

Initial Temp. T_{init}, K	**First - stage ignition**		**First-stage Conclusion**		**Second - stage ignition**	
	(τ_1), s	**T_1, K**	**(τ_{1A}), s**	**T_{1A}, K**	**(τ_2), s**	**T_2, K**
1000	-	-	-	-	0.044	1908
950	-	-	-	-	0.104	1865
900	-	-	-	-	0.266	1859
850	-	-	-	-	0.677	1810
825	-	-	-	-	0.997	1812
800	-	-	-	-	1.278	1802
775	0.054	777	0.366	792	1.321	1786
750	0.017	760	0.254	785	1.198	1780
725	0.015	750	0.067	784	0.99	1756
700	0.021	748	0.067	792	0.759	1736
675	0.038	751	0.079	804	0.569	1720
650	0.081	759	0.122	817	0.461	1716
625	0.199	766	0.237	829	0.478	1690
600	0.569	772	0.599	839	0.784	1682
550	7.445	777	7.461	851	7.599	1661
525	35.39	773	35.41	853	35.53	1649
500	215.6	768	215.69	851	215.81	1625
475	1849	761	1849	846	1849.3	1625
450	26632	753	26633	840	26633	1616

Table 3.1. Ignition delay times, and corresponding ignition temperatures for initial mixture temperatures ranging from 450 – 1000 K

While other models exhibit comparable behavior, the UCSD mechanism demonstrates a distinctly unique behavior. Figure 3.4 shows a representative three-stage ignition process of stoichiometric gas mixture of *n*-heptane/air under initial temperature of 450 K and atmospheric pressure (101325 Pa). The three distinct peaks in the rate of temperature rise correspond to temperature-dependent chain-branching reactions of low temperature chemistry (LTC), intermediate temperature chemistry (ITC), and high temperature chemistry (HTC). These distinct chemical regimes, originating from varied chain-branching pathways, result in flames characterized as cool flames (LTC), warm flames (ITC), and hot flames (HTC). In this context, the first-stage ignition delay time (τ_1) is 3041.14 s, while the second-stage ignition delay time (τ_2) is 3014.51 s. The period from the simulation's onset to the ignition of the warm flame, denoted as τ_{WF}, is 3014.43 s.

The 'x' marks positioned just beyond the cool and warm flame ignition points, indicate the end of each ignition stage, and mark the local minimum in the rate of temperature change (dT/dt). The ignition temperatures for the cool, warm, and hot flames are approximately 663 K, 789 K, and 1622 K, respectively. Notably, warm flames, which are part of an LTC-ITC structure, can only exist outside the established flammability limits of lean and rich hot flames. However, further research is necessary to delineate their precise occurrence, limits, and how they affect cool and hot flame ignition.

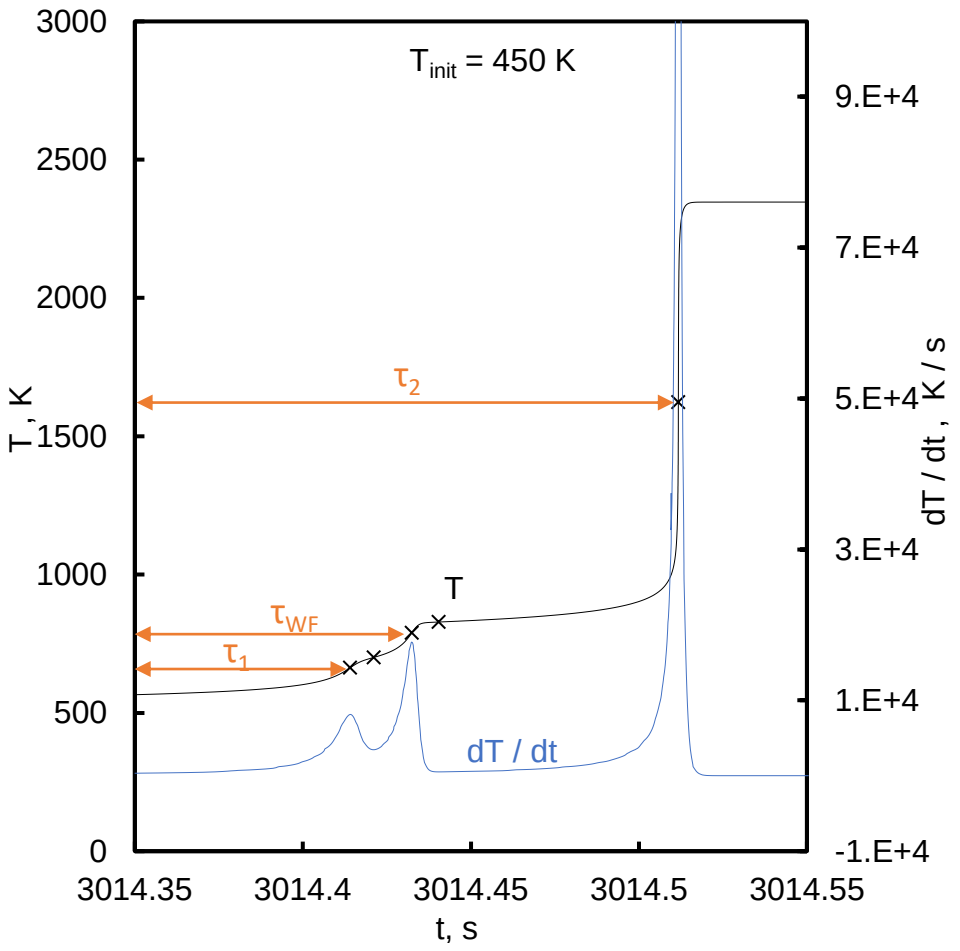

Figure 3.4. Temperature versus time history for *n*-heptane/air mixture at atmospheric pressure and initial mixture temperature of about 450 K. This is an example of a three-stage ignition process

3.2 Species composition

Figure 3.5 shows the temperature versus time behavior and the simulated mole fraction profiles for carbon dioxide (CO_2), nitrogen (N_2), and oxygen (O_2) generated using the CRECK mechanism for a stoichiometric *n*-heptane/air gas mixture at atmospheric pressure (101325 Pa), for initial mixture temperature of 650 K. The mole fraction of unburned fuel has also been included in the plot to depict the fuel consumption at the two ignition stages.

The plot reveals that during the cool flame phase at 0.08 s, there is a small rise in temperature accompanied by a significant production of CO_2. Later, the mixture continues to heat until a hot ignition is triggered at 0.46 s. At this point a large amount of CO_2 is generated. It is interesting to note that at the cool flame stage, only a fraction of total unburned fuel is consumed, while the hot ignition phase sees the complete combustion of the remaining fuel.

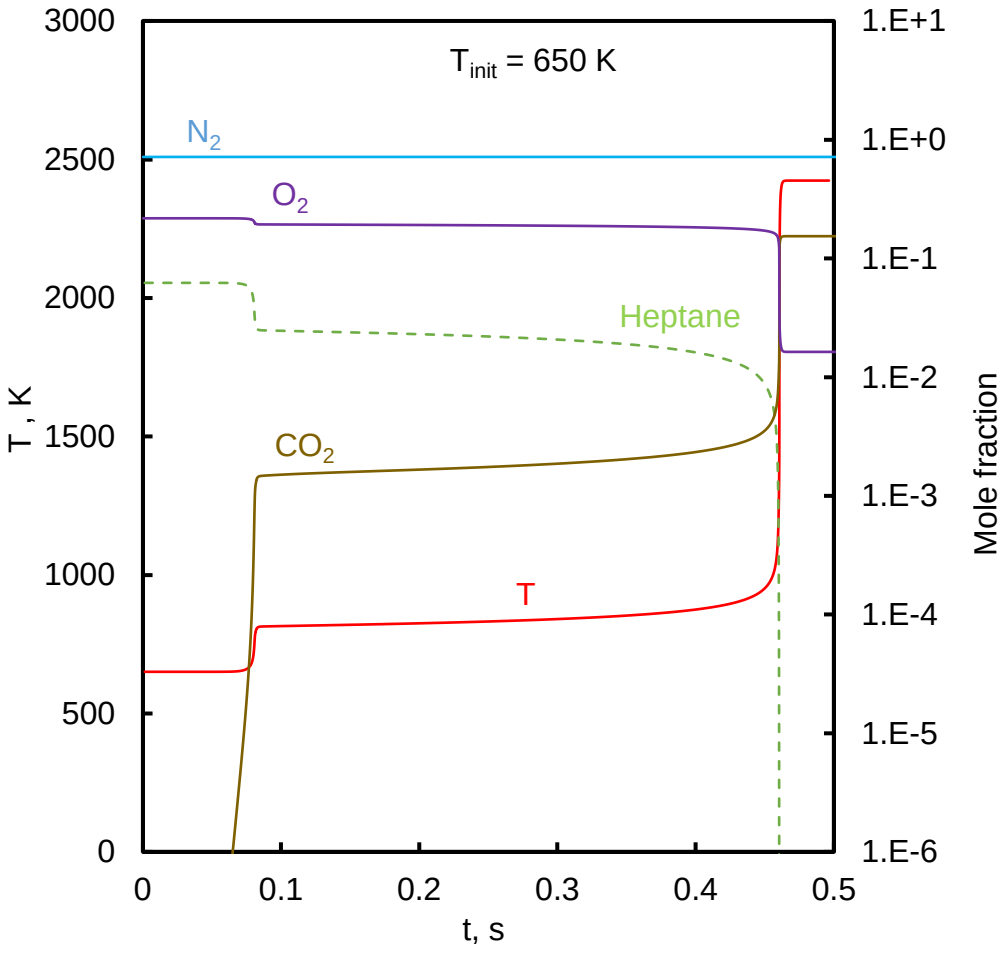

Figure 3.5. Simulated mole fractions for CO_2, O_2, N_2, and heptane for a stoichiometric *n*-heptane/air gas mixture at atmospheric pressure under initial mixture temperature of 650 K

The plot also depicts that the N_2 concentration remains constant as witnessed by a straight line, indicating its abundance throughout the simulation. Additionally, only a minor amount of oxygen is utilized during the cool flame phase, with a substantially larger consumption occurring during the hot ignition phase.

Fig 3.6 shows the temperature versus time behavior and the simulated mole fraction profiles for water (H_2O), formaldehyde (CH_2O), hydroperoxy radical (HO_2), and a keto-hydroperoxide (KHP) species $C_7H_{15}OOH$ generated using the CRECK mechanism for a stoichiometric *n*-heptane/air gas mixture at atmospheric pressure (101325 Pa), for initial mixture temperature of 650 K.

Fig 3.7 shows the temperature versus time behavior and the simulated mole fraction profiles for carbon monoxide (CO), hydrogen peroxide (H_2O_2), and hydroxyl radical (OH) generated using the CRECK mechanism for a stoichiometric *n*-heptane/air gas mixture at atmospheric pressure (101325 Pa), for initial mixture temperature of 650 K.

From the plot it can be observed that prior to the first stage of ignition, a sequence of pre-ignition reactions build a pool of keto-hydroperoxide (KHP) species that play a major role in the first-stage ignition. These KHP species further decompose but below 800 K the production rate is higher than the decomposition rate, leading to build up of a KHP pool.

Decomposition of the RO_2 and KHP molecules produces OH and other radicals that further attack the parent fuel molecules. At this stage, various oxidation reactions involving radical species and hydrocarbon fragments raise the temperature and the heat release peaks at this time.

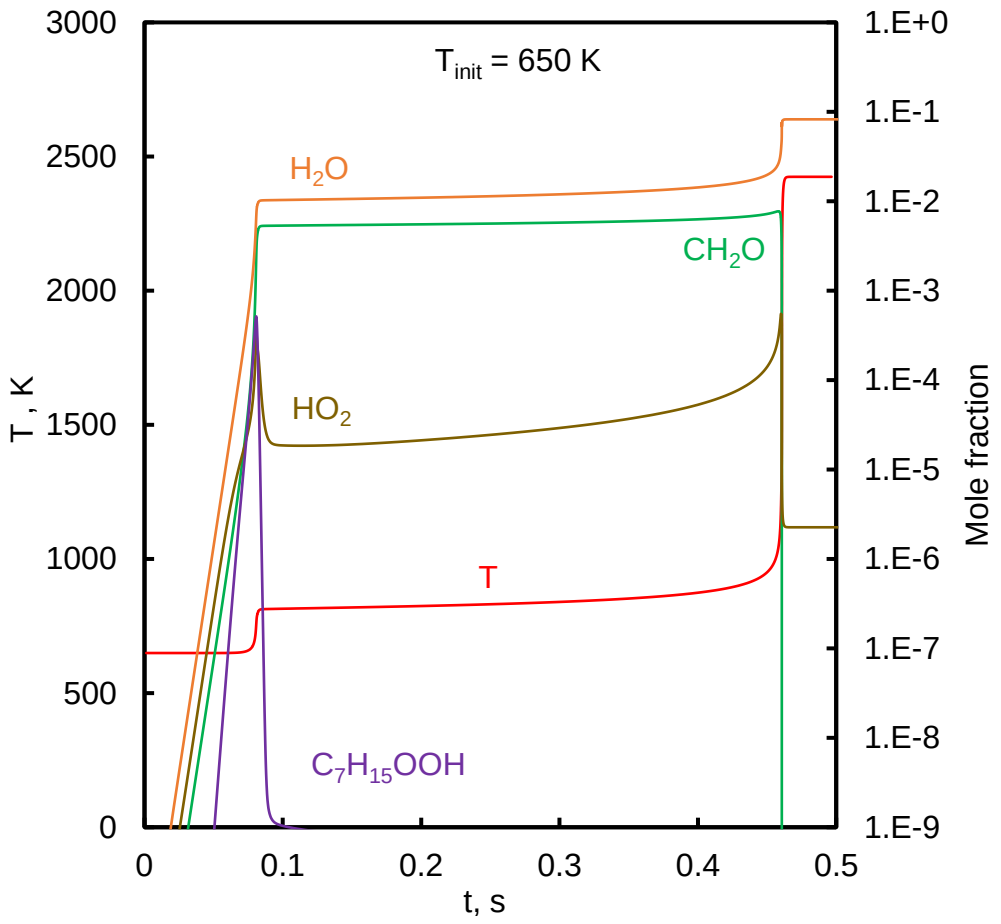

Figure 3.6. Simulated mole fractions for H_2O, CH_2O, HO_2, and $C_7H_{15}OOH$ for a stoichiometric *n*-heptane/air gas mixture at atmospheric pressure under initial mixture temperature of 650 K

When the temperature nears 850 K, the chemical equilibrium of the reaction between R and O_2 alters, resulting in a decrease in RO_2 production. This change hampers the series of reactions responsible for accumulating the ketohydroperoxide (KHP) pool. Similarly, at these elevated temperatures, the equilibrium of the subsequent reaction involving the addition of O_2 is inclined towards breaking apart the molecules, which further impedes the formation of KHP.

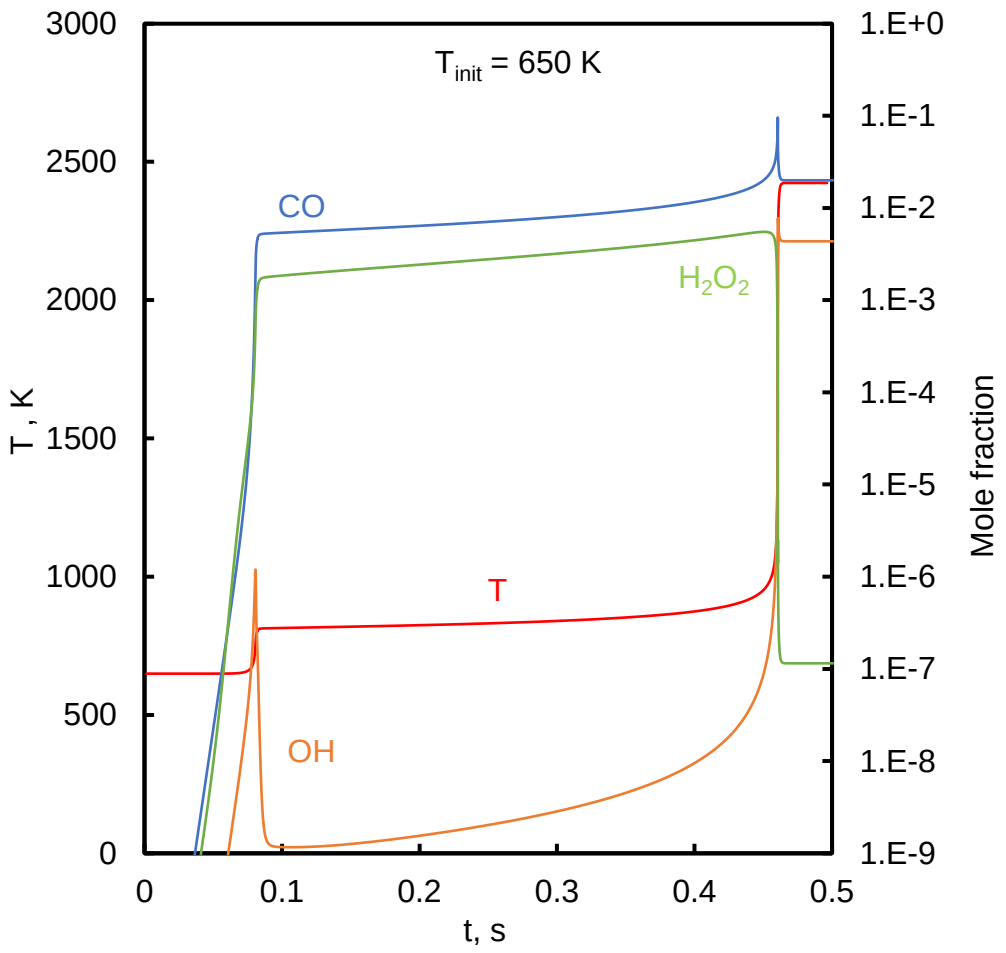

Figure 3.7. Simulated mole fractions for H_2O_2, CO, and OH for a stoichiometric *n*-heptane/air gas mixture at atmospheric pressure under initial mixture temperature of 650 K

The first stage of ignition ends when the temperature rises sufficiently that the KHP pool is depleted. It is this rapid depletion of the KHP pool that leads to the so-called "negative temperature coefficient" regime, wherein heat release rates slow despite increasing temperature.

During the second-stage pre-ignition, pools of H_2O_2 and CO build as the formaldehyde (CH_2O) formed during the first stage is gradually oxidized and also by the combination of hydroperoxy radicals (HO_2) that are formed during the first stage

of ignition, along with other unburned hydrocarbons. At the same time it is being formed, some H_2O_2 decomposes into OH radical species, but until the temperature reaches 1000 K, the production reactions outweigh decomposition, and the H_2O_2 pool continues to build. . As the available pool of OH and other species continues to oxidize unburned hydrocarbon species, the temperature gradually rises.

When the temperature has increased sufficiently, the H_2O_2 decomposition exceeds production, releasing a pool of OH radicals that initiate a high-temperature second-stage ignition, where most of the formaldehyde, CO, and unburned hydrocarbon are consumed and where OH is formed in abundance. Table 3.2 shows the ignition characteristics and mole fractions for fig 3.5 – 3.7.

Component	**First-stage ignition**	**Second-stage ignition**	**Peak**
Delay Time (s)	0.080	0.460	-
Ignition Temp. (K)	758.83	1716.27	-
Mole Fraction			
C_7H_{16}	3.34 E-02	6.99 E-20	6.22 E-02
CO_2	7.92 E-04	2.88 E-02	1.54 E-01
O_2	2.01 E-01	1.93 E-01	2.19 E-01
N_2	7.19 E-01	7.19 E-01	7.19 E-01
H_2O	6.80 E-03	7.01 E-02	8.22 E-02
CH_2O	2.45 E-03	3.94 E-04	7.69 E-03
HO_2	3.14 E-04	8.85 E-05	5.50 E-04
$C_7H_{15}OOH$	5.14E-04	9.07E-10	5.15E-04
H_2O_2	5.83 E-04	1.50 E-06	5.51 E-03
CO	2.17 E-03	9.42 E-02	9.51 E-02
OH	1.19 E-06	2.17 E-03	7.78 E-03

Table 3.2. Ignition characteristics and key species composition for a two-stage ignition process of n-heptane/air at atmospheric pressure under initial temperature of 650 K

3.3 *Negative – Temperature Coefficient (NTC) behavior*

Figure 3.5 shows the computed ignition delay time (τ) as a function of initial mixture temperature (T_{init}), as summarized in Table 3.1, for a stoichiometric gas mixture of *n*-heptane/air at atmospheric pressure (101325 Pa), for initial mixture temperatures of 450 – 1000 K.

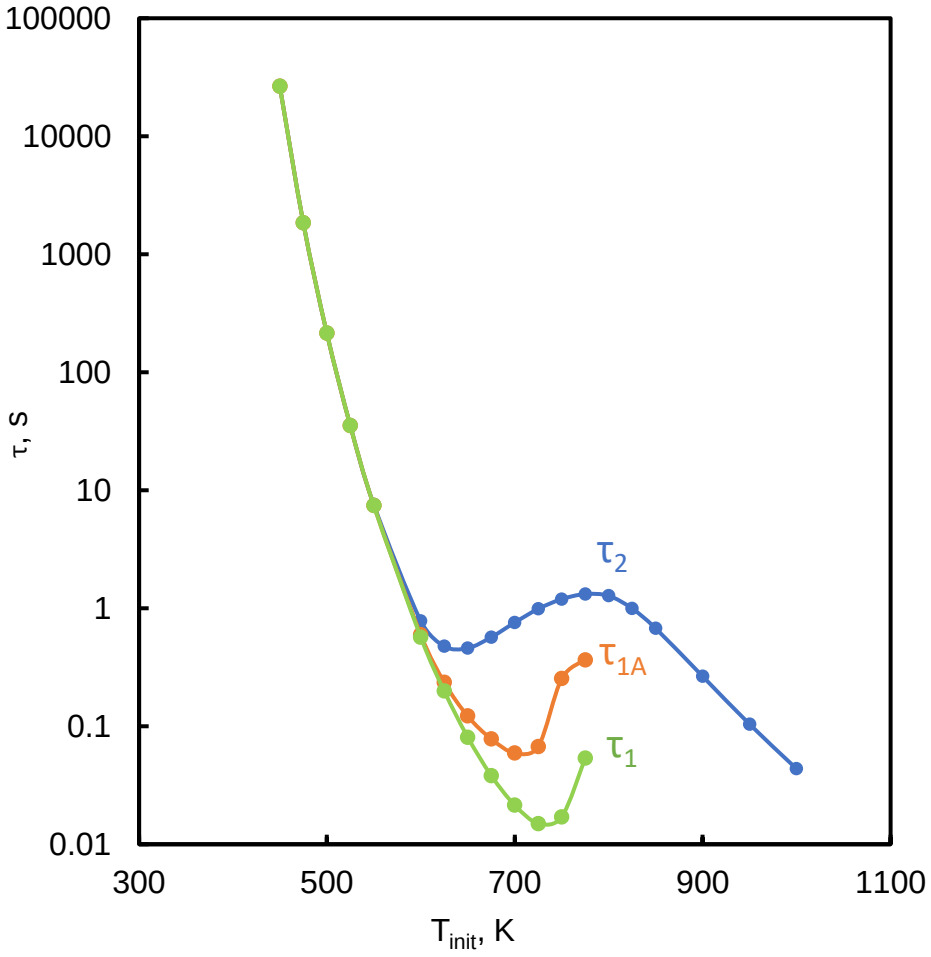

Figure 3.8. NTC responses for a stoichiometric *n*-heptane/air mixture at atmospheric pressure. The first-stage ignition delay time (τ_1) is indicated by a solid green line, the first-stage ignition conclusion time (τ_{1A}) is denoted by a solid orange line, and delay time for the second-stage ignition (τ_2) is marked by a solid blue line

From the plot, it is observed that for either sufficiently low temperatures (below 625 K) or sufficiently high temperatures (above 775 K), the second-stage ignition delay time (τ_2) decreases with an increase in mixture temperature. However, in contrast, within the intermediate temperature range (625 – 775 K), τ_2 exhibits an increase as the temperature rises. Similarly, the first-stage ignition delay time (τ_1) and the termination time of the first-stage ignition (τ_{1A}) both initially decrease and then increase with increasing mixture temperature, demonstrating their own response in transition to the intermediate temperature regime. This region of non-monotonic mixture reactivity is termed the Negative – Temperature Coefficient (NTC) region and is fundamentally responsible for the existence of stable cool flames. A combination of low and high temperature chemistry is needed to simulate this NTC behavior.

It is evident that the ignition delay time for both first and second-stage ignition generally decreases with an increase in the initial mixture temperature, T_{init}. However, this trend is interrupted within the NTC regime, characterized by specific threshold temperatures known as the lower and upper "turnover temperatures". Outside these threshold temperatures, the ignition delay recommences its decrease with rising initial mixture temperatures. Understanding the nuances of these turnover temperature boundaries, often referred to as turnover states, is essential. They demarcate the transitions between low-to intermediate and intermediate-to-high temperature boundary within the NTC regime. Developing a scaling for these turnover temperature limits can significantly diminish uncertainties and furnish a more accurate benchmark for selecting experimental data pertinent to specific experimental conditions.

The lower turnover temperature (T_{lower}) represents the minimum temperature at which the NTC behavior commences, while the upper turnover temperature (T_{upper}) indicates the maximum temperature limit for these reactions above which the NTC behavior vanishes.

Figure 3.6 illustrates the relationship between ignition delay times and temperatures in proximity to both the lower and upper turnover temperatures. This plot is utilized to determine the lower upper turnover temperature based on the ignition delay data presented in fig. 3.5.

The NTC curve displays a sophisticated pattern where the concavity alternates between downward and upward, rather than following a simple increase or decrease. To capture this non-linear variation, the curve was investigated using a cubic fitting approach employing a third-degree polynomial, as it accommodates an inflection point where the curvature's trajectory alters. This makes it a more precise model compared to a second-degree polynomial. Moreover, the R-squared value is one, signifying that the cubic model accounts for almost all the variation in the response data about its average.

To identify the temperatures where the concavity of the NTC curve shifts, termed the lower and upper turnover temperatures (T_{lower} and T_{upper}), the cubic equations obtained from the third-order polynomial fit were analyzed, as displayed in fig. 3.6. This analysis is conducted using calculus, initially by calculating the first derivative of the equation, followed by determining the roots of the equation. Upon resolving the equations, it was determined that the lower turnover temperature occurs

at 640 K with a corresponding time of 0.44 seconds, while the upper turnover temperature is identified at 783 K, occurring at 1.33 seconds.

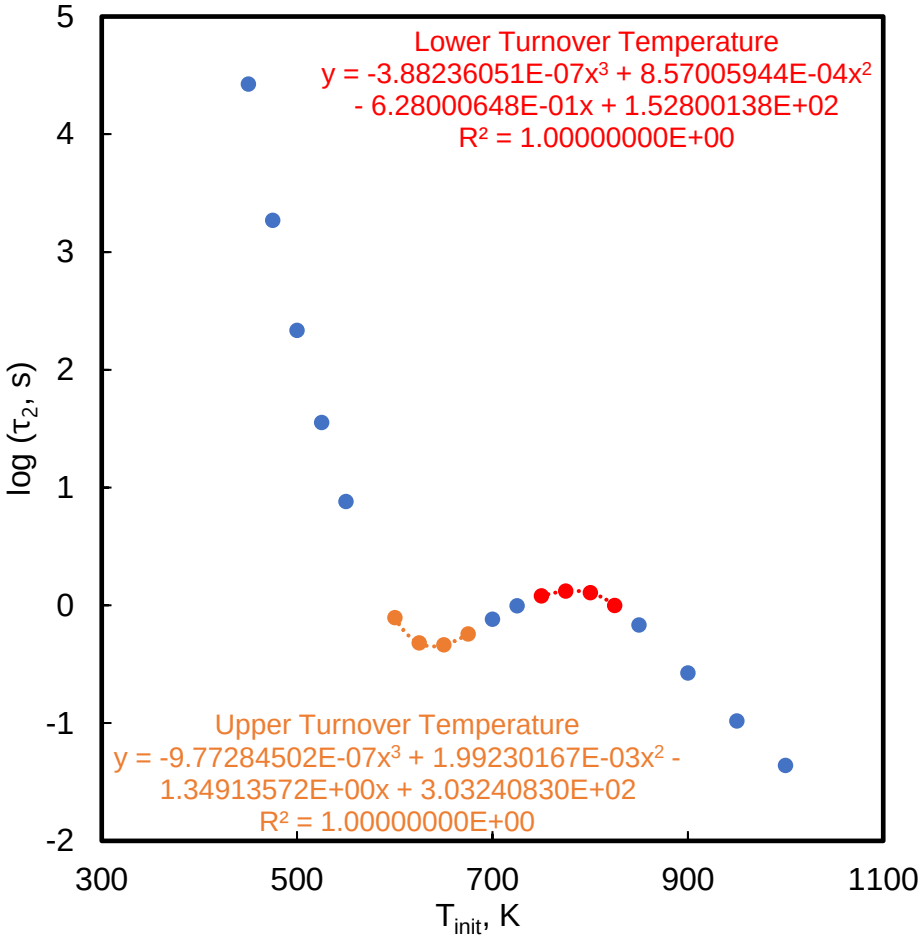

Figure 3.9. Variation of logarithmic second – stage ignition delay time with initial mixture temperature. The dataset is fitted using a cubic polynomial covering the points near the lower and upper turnover temperature

Interestingly, there is a critical temperature where the phenomenon of two-stage ignition ceases, leading to the disappearance of the temperature increase and leaving only a single stage ignition. This critical temperature is referred to as the crossover temperature, symbolized by T*. It represents the point at which the heat release from the first stage ignition becomes negligible. This critical temperature is determined by

averaging the highest initial mixture temperature at which two-stage ignition occurs and the subsequent temperature where only single-stage ignition is observed. This calculation is demonstrated in Eq. (3.3).

$$T^* = \frac{T_{two-stage} + T_{single-stage}}{2} \tag{3.3}$$

Where,

T* represents the crossover temperature

$T_{two\text{-}stage}$ is the highest initial mixture temperature at which two-stage ignition is present. $T_{single\text{-}stage}$, is the temperature right after, $T_{two\text{-}stage}$ where only single-stage ignition is present.

Here, $T_{two\text{-}stage}$ is 775 K, while $T_{single\text{-}stage}$ is 800 K, utilizing the equation, the crossover temperature is determined to be 788 K. Figure 3.7. represents the computed lower and upper turnover temperature and crossover temperature. It can be observed that the crossover temperature is quite close to the upper turnover temperature. Therefore, the crossover temperature also corresponds to the transition of chemistry from low- to intermediate-to-high temperature regime.

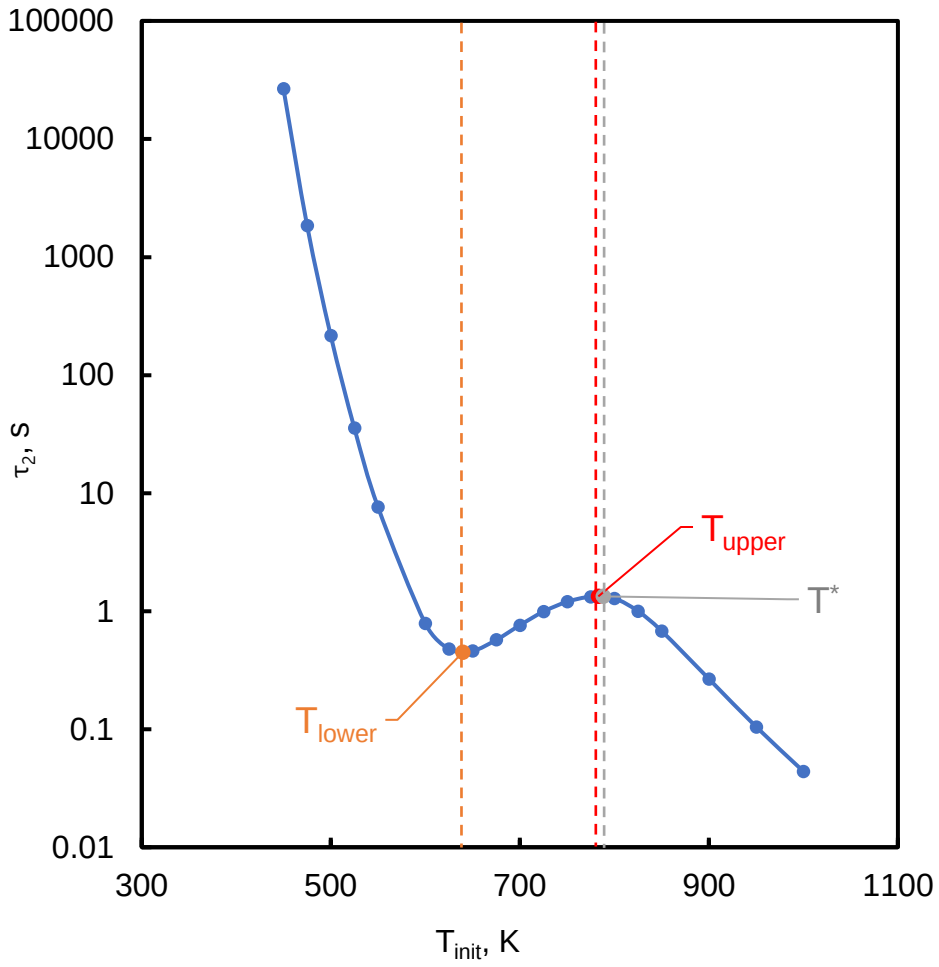

Figure 3.10. The lower turnover (T_{lower}), upper turnover (T_{upper}), and crossover temperature (T^*) for a stoichiometric *n*-heptane/air mixture

Cool diffusion flames necessitate the presence of a Negative Temperature Coefficient (NTC) region and are exclusively present during the period from the onset of first-stage ignition to the conclusion of first-stage ignition. Figure 3.11 illustrates the relationship between the initial mixture temperatures and the temperatures at the beginning (T_1) and end (T_{1A}) of first-stage ignition. The dashed box denotes the temperature range for the cool flames. The initial mixture temperature i.e., the lower and upper turnover temperature is 640 – 775 K while the minimum ignition temperature is 747 K, and the maximum ignition temperature is 822 K.

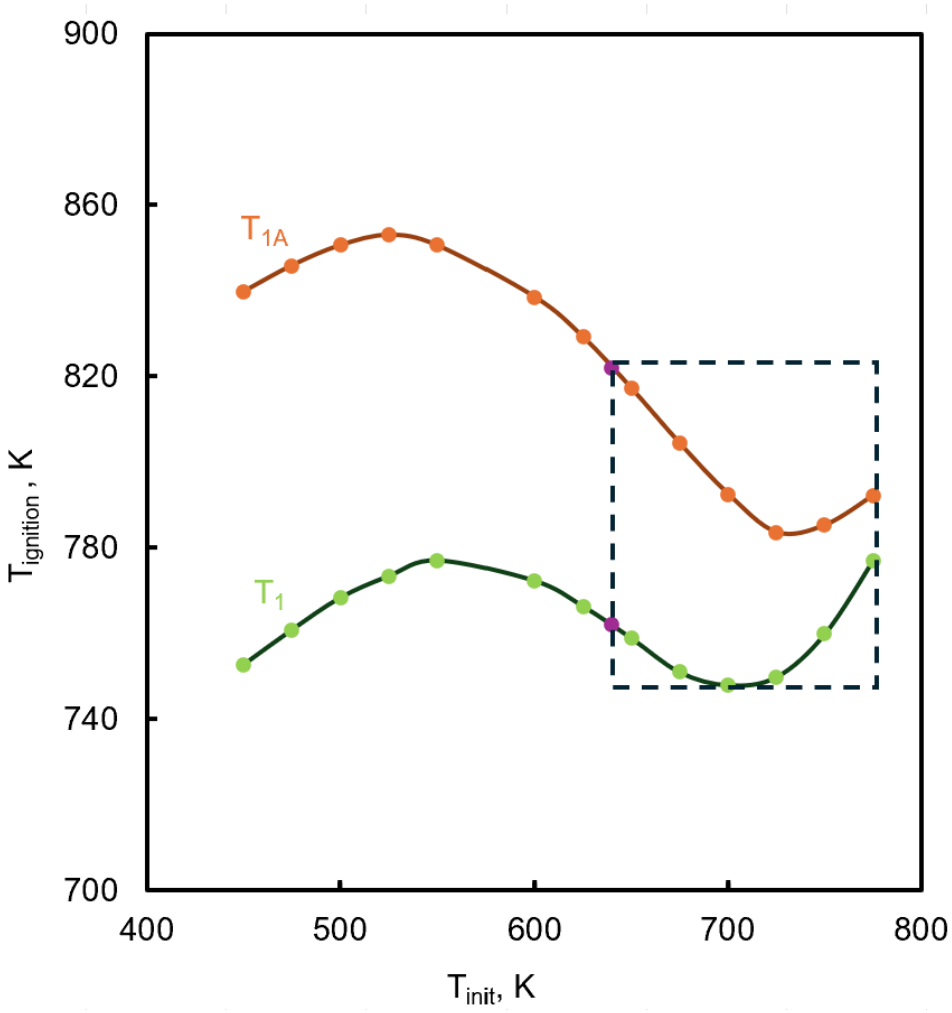

Figure 3.11. First-stage ignition and first-stage ignition conclusion temperature as a function of initial mixture temperature

Figure 3.8. shows the variation of logarithmic second-stage ignition delay time with inverse initial mixture temperature. It can be observed that the low and high-temperature portion of the curve can be well represented by an Arrhenius expression. Using the Arrhenius expression, the activation energy in the lower and upper turnover state regime can be determined.

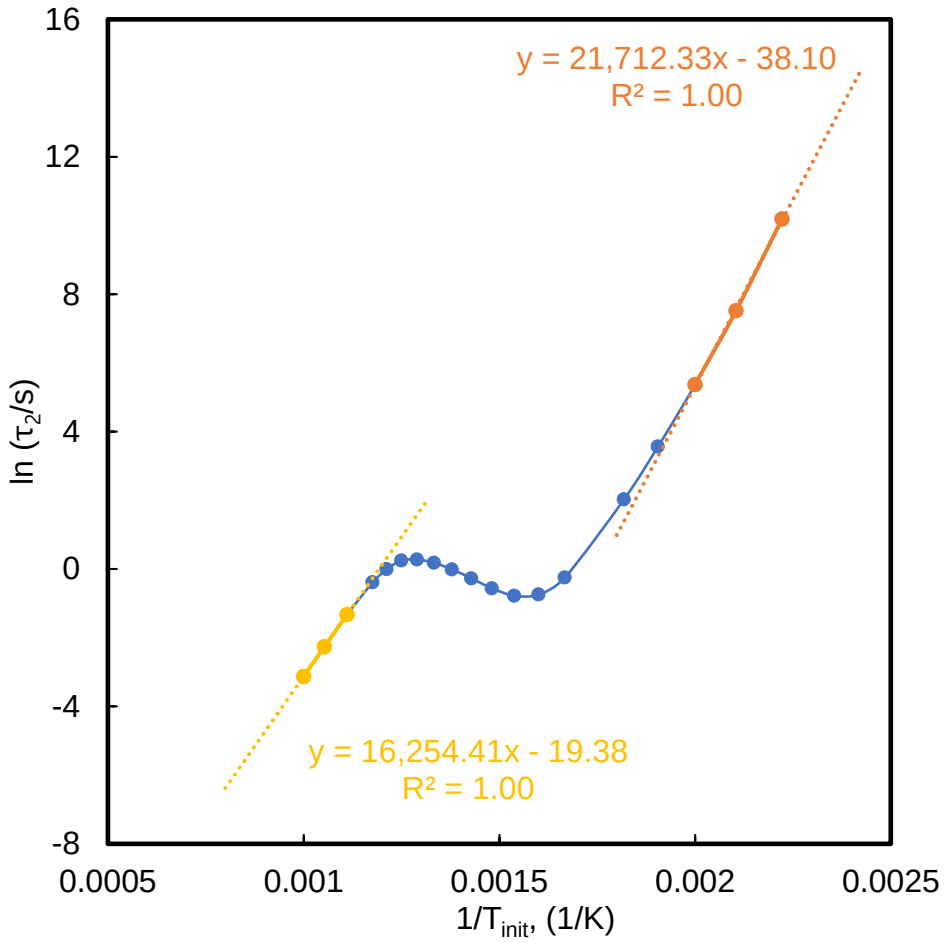

Figure 3.12. Variation of logarithmic second-stage ignition delay time with inverse of initial mixture temperature exhibiting Arrhenius behavior. The high and low temperature segments of the curve are represented by yellow and orange lines, respectively, and the slopes of these segments have been used to calculate the activation energy

In the process of analyzing the temperature dependence of reaction rates, we utilize the Arrhenius equation to derive the activation energy. The starting point is a linear equation obtained from plotting the negative temperature coefficient for initial temperatures of 450, 475 and 500 K. This yields the following relationship.

$$ln\left(\frac{\tau_2}{s}\right) = 21{,}712\frac{1}{T} - 38.09 \tag{3.4}$$

The Arrhenius equation, is given by:

$$k = Ae^{\frac{-E_a}{RT}} \tag{3.5}$$

where,

k denotes the rate constant

A is the pre-exponential factor

E_a is the activation energy (in J/mol)

R is the universal gas constant (8.314 J/mol.K)

T is the temperature (in Kelvin)

For graphical analysis and better comprehension of the relationship between the rate constant and temperature Eq. 3.5. is linearized by taking the natural logarithm of both sides.

$$\ln(k) = -\frac{E_a}{R}\frac{1}{T} + \ln(A) \tag{3.6}$$

This transformation facilitates the direct comparison of Eq. 3.4 against the Arrhenius model. $ln\left(\frac{\tau_2}{s}\right)$ corresponds to $\ln(k)$. The slope of the equation corresponds to $-\frac{E_a}{R}$ and the intercept corresponds to $\ln(A)$.

Identification of these parameters allows for the computation of the activation energy (Ea) from the slope.

$$-\frac{E_a}{R} = \text{Slope} \tag{3.7}$$

$$E_a = -Slope * R \tag{3.8}$$

$$E_a = -(21{,}712\ k^{-1}) * 8.314\ \frac{Joules}{mol * K}$$

$$E_a = 180{,}516.33\ J/mol$$

Similarly, the activation energy (Ea) near the higher temperature portion of the curve for initial temperatures of 900, 950 and 1000 K is 135,138.20 J/mol.

3.4 Effect of equivalence ratio on the NTC behavior

To explore the effect of equivalence ratio on the Negative Temperature Coefficient (NTC) behavior and threshold temperatures, mixture compositions ranging from 'lean' to 'rich' were analyzed using the CRECK mechanism. Figure 3.12 shows the computed second-stage ignition delay time (τ_2), for a *n*-heptane/air gas mixture at atmospheric pressure (101325 Pa), for initial mixture temperature of 450 – 1000 K at an equivalence ratio of 0.5, 1, 2, 4, 8, 16, and 32.

From the plot it can be observed that all the mixture compositions from 'lean' to 'rich' exhibit NTC behavior. It is interesting to note that for initial mixture temperatures of 650 – 1000 K, the minimum ignition delay time was exhibited at the richest mixture composition i.e., at an equivalence ratio of 32. Within the specified temperature range, a progressive increase in the equivalence ratio starting from 0.5 led to a consistent decrease in the ignition delay time. However, this trend was interrupted within the temperature range of 450 – 600 K. For instance, the minimum ignition delay time at T_{init} of 450 K was found to be exhibited at stoichiometric conditions.

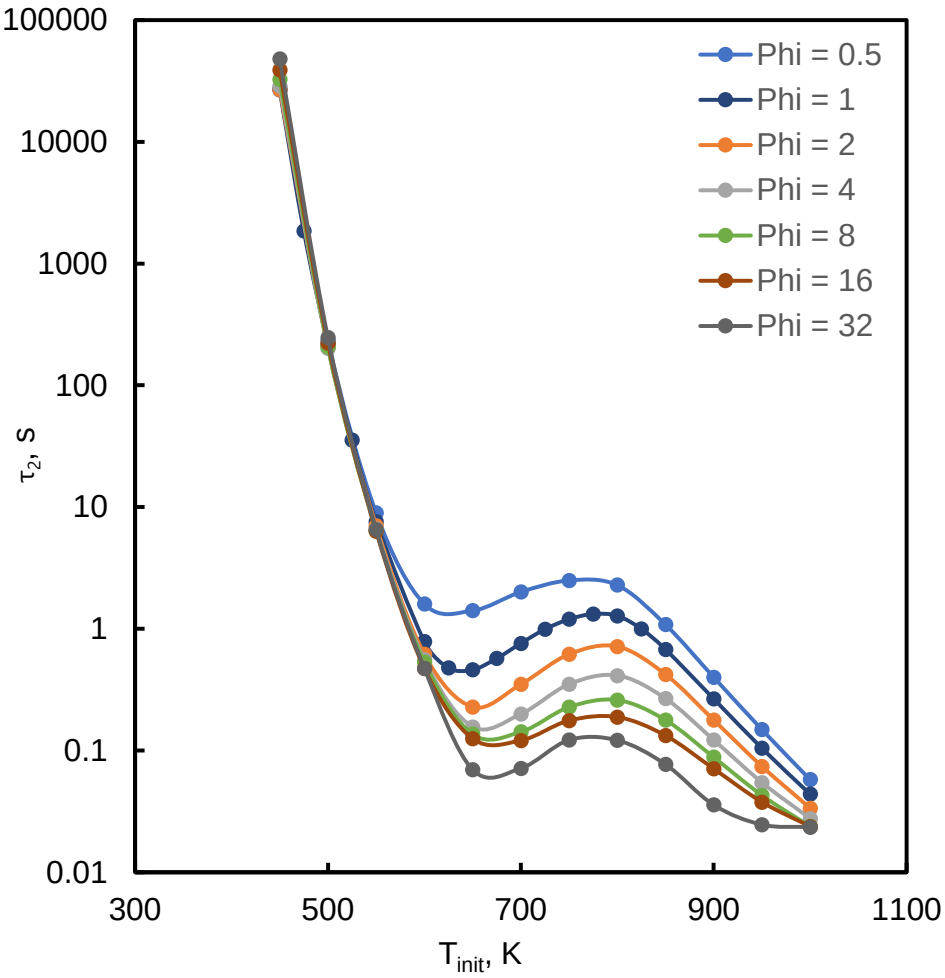

Figure 3.13. NTC responses of second – stage ignition delay time (τ_2) for *n*-heptane/air gas mixture at atmospheric pressure across equivalence ratio 0.5 – 32

To gain a deeper insight into how the equivalence ratio impacts the species composition, simulations with fixed time stepping were conducted at an initial mixture temperature of 650 K, employing the CRECK mechanism. Figure 3.13 shows the mole fraction profile of oxygen with respect to time, Fig. 3.14 shows the mole fraction profile of heptane with respect to time, Fig. 3.15 shows the mole fraction profile of hydrogen peroxide with respect to time and Fig. 3.16 shows the mole fraction profile of formaldehyde with respect to time for equivalence ratio of 0.5 – 32.

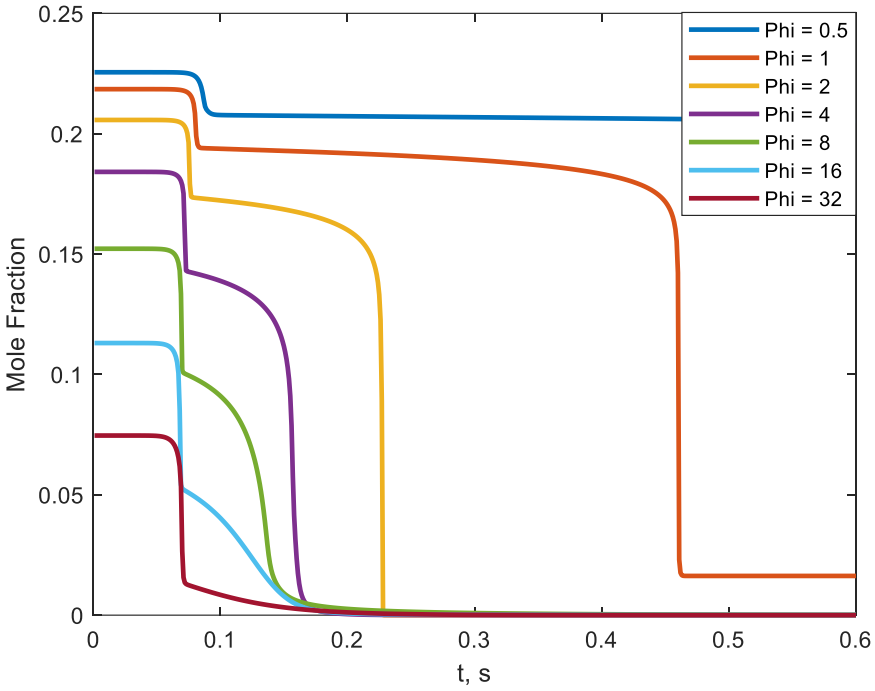

Figure 3.14. Simulated mole fraction profile of oxygen with respect to time for an equivalence ratio of 0.5 – 32

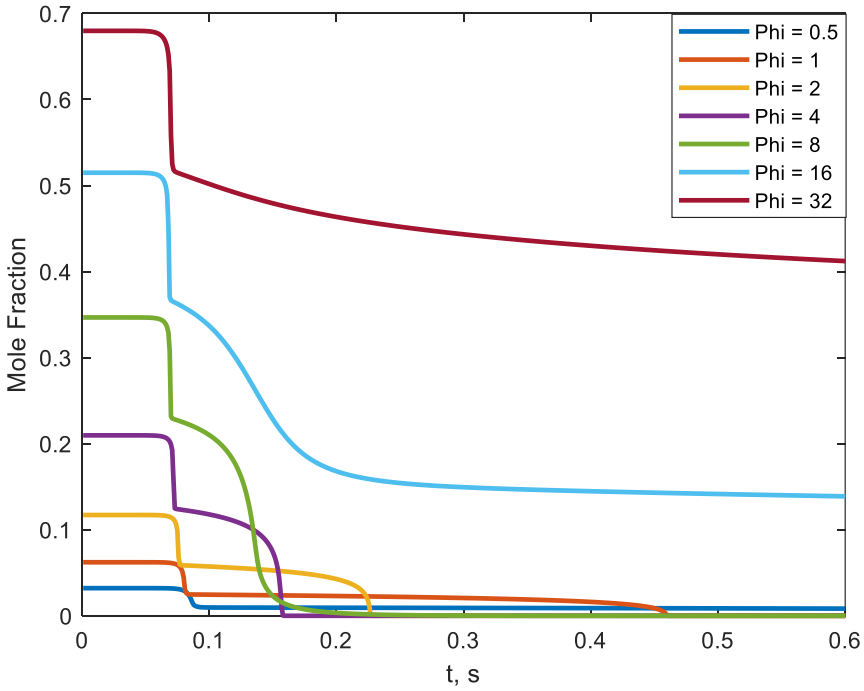

Figure 3.15. Simulated mole fraction profile of *n*-heptane with respect to time for an equivalence ratio of 0.5 – 32

From fig. 3.13 and 3.14 it is clear that the timing of first-stage ignition is nearly the same for all mixture compositions while there is a significant timing difference in the location of the second-stage ignition, which is strongly affected by the mixture stoichiometry. It is evident that rich mixtures achieve second-stage ignition much faster post the first-stage ignition process than leaner mixtures. This is due, at least in part, to the increased temperature rise that occurs during the first stage ignition. For instance, the temperature at the first-stage ignition conclusion at an equivalence ratio of 0.5 is 782 K, while at an equivalence ratio of 8 is 865 K. As we move to further richer mixtures, for example at an equivalence ratio of 32, the energy needed to break apart fuel molecules quickly soaks up heat and the temperature falls steeply to 822 K. Hence, with increasing equivalence ratio, the temperature at the end of the first stage ignition keeps increasing and is already approaching the temperature at which rapid H_2O_2 decomposition occurs.

The predicted influence of equivalence ratio on formaldehyde is also important. Figure 3.16 shows that formaldehyde is formed at the first-stage of ignition when the KHP pool decomposes and persists until is destroyed at the second-stage of ignition. Formaldehyde exists during the dwell between the two stage of ignition, the length of which depends on the mixture stoichiometry.

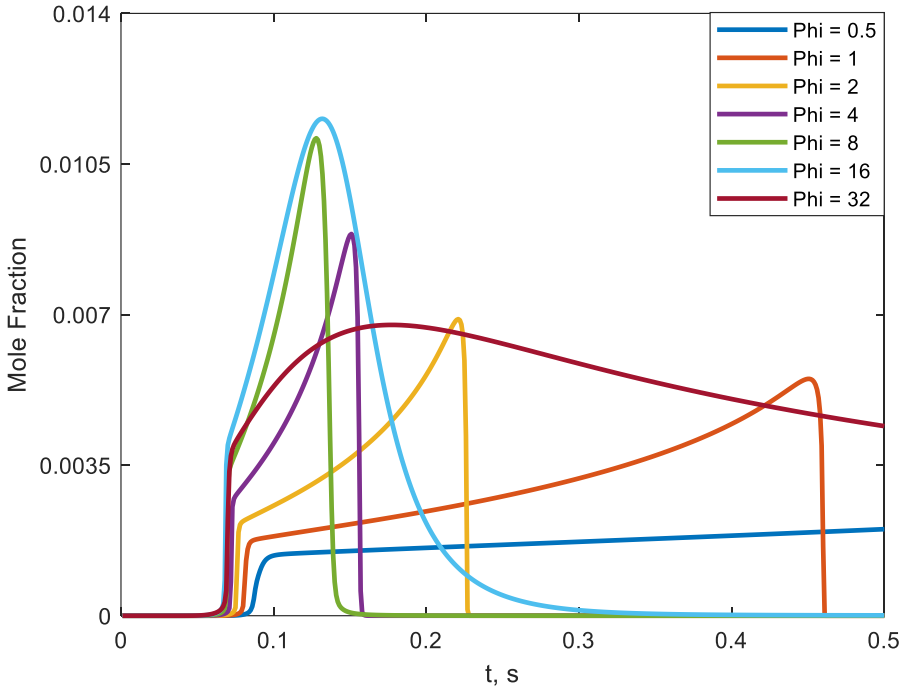

Figure 3.16. Simulated mole fraction profile of hydrogen peroxide with respect to time for an equivalence ratio of 0.5 – 32

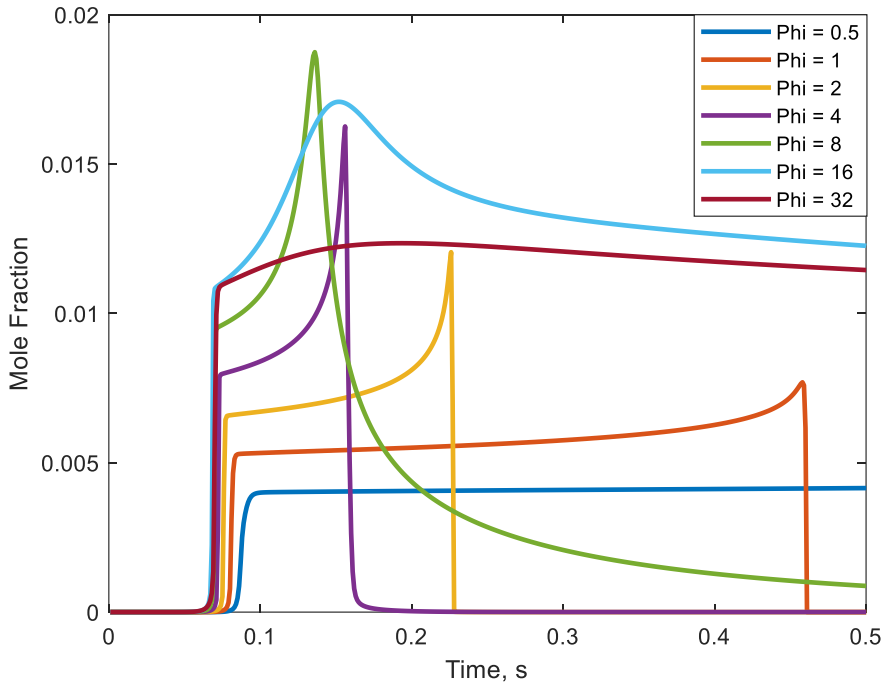

Figure 3.17. Simulated mole fraction profile of formaldehyde with respect to time for an equivalence ratio of 0.5 -32

To further investigate the temperature range of the NTC phenomenon, i.e., the lower and upper turnover temperature, a cubic fitting approach using a third-degree polynomial as described in section 3.3 has been employed for each equivalence ratio. However, this approach was unable to resolve the temperature thresholds for an equivalence ratio of 32. Table 3.3 lists out the lower and upper turnover temperature and the range ($T_{upper} - T_{lower}$) of the NTC region.

Phi	Lower Turnover T_{lower}	Upper Turnover T_{upper}	Turnover Range $T_{upper} - T_{lower}$, K
0.5	629	767	138
1	639	783	144
2	653	789	136
4	662	792	129
8	671	791	120
16	679	783	104

Table 3.3. Lower and upper turnover temperature and the turnover range for equivalence ratio 0.5 - 16

From the table, it is evident that as the equivalence ratio increases, the cool flame range tends to decrease. Hence, for a much wider range for cool diffusion flames, it is essential to exist at or near stoichiometric conditions.

3.5 Impact of different chemical kinetic mechanisms on the NTC behavior

To develop a more comprehensive understanding of the Negative Temperature Coefficient (NTC) behavior and its metric, specifically the lower and upper turnover temperature thresholds, several of the most commonly used kinetic mechanisms reported in the literature were evaluated. Table 3.2 presents six different chemical kinetic mechanisms utilized to compute the ignition delay times for a stoichiometric *n*-heptane/air gas mixture at atmospheric pressure (101325 Pa), with initial mixture

temperature of 475 – 1000 K. The pathways and reaction rate parameters of these mechanisms are extensively detailed in their respective publications.

Kinetic Mechanism	Institution	Species count	Reaction count	Reference
High plus low temp. (HT+LT)	CRECK [46]	339	9781	[52]
Detailed Mechanism Version 3	LLNL [47]	654	2827	[53]
n-Heptane Mechanism	NUIG [48]	1268	5336	[54]
Complete San Diego Mechanism with Heptane Chemistry	UCSD [49]	57	268	[55]
Detailed Chemical Kinetic Model	CALTECH [50]	194	1156	[56]
Jerzembeck Detailed Mechanism	CERFACS [51]	203	1001	[57]

Table 3.4. List of chemical kinetic mechanisms used to calculate ignition delay times for a stoichiometric n-heptane/air mixtures at atmospheric pressure

The number of species and reaction count has a significant effect on the computational time of the simulation.

Figure 3.12 shows the computed second-stage ignition delay time as a function of initial mixture temperature (T_{init}) for the six mechanisms outlined above, all of which successfully captured the NTC behavior. An increase in T_{init} led to a reduction in ignition delay time across all mechanisms. However, as previously mentioned this trend was interrupted within the NTC regime, particularly at the lower and upper turnover thresholds.

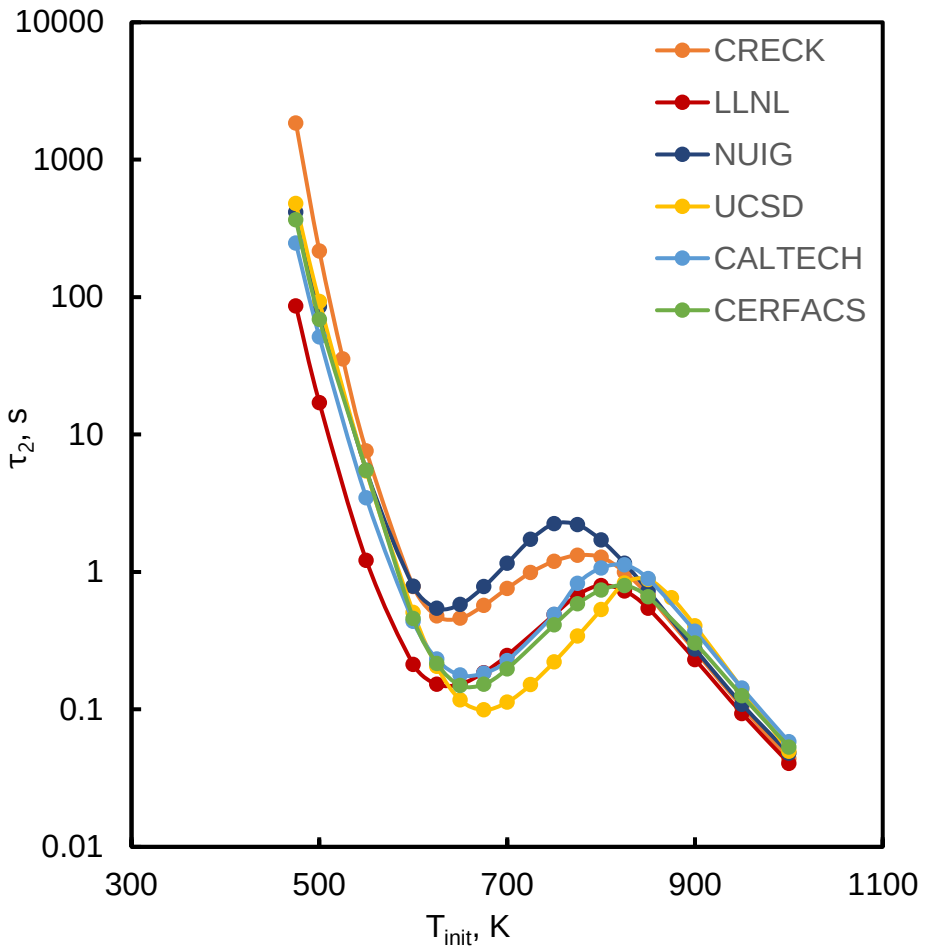

Figure 3.18. NTC response of different chemical kinetic mechanisms outlined in Table 3.2. for a stoichiometric n-heptane/air mixture at atmospheric pressure

It is noteworthy that, at higher T_{init}, the ignition delay times across all mechanisms tend to converge. Yet, at cooler temperatures, they do not match up as well. Specifically, at a T_{init} of 475 K, the ignition delay time for the CRECK mechanism was 1849.34 s, in contrast to the LLNL mechanism, which was 86.28 s, indicating a substantial deviation of about 2043 %. The same discrepancy can also be witnessed within the intermediate temperature range i.e., the turnover temperature thresholds.

Fig. 3.12 shows the lower and upper turnover temperature thresholds for all six mechanisms, calculated using the same cubic fitting method described in section 3.3, which utilizes a third-degree polynomial. The LLNL mechanism exhibits the minimum lower turnover temperature at 636.81 K, whereas the maximum upper turnover temperature is 841.68 K, as demonstrated by the UCSD mechanism. The mean lower turnover temperature is 653 K, while the mean upper turnover temperature is 804 K.

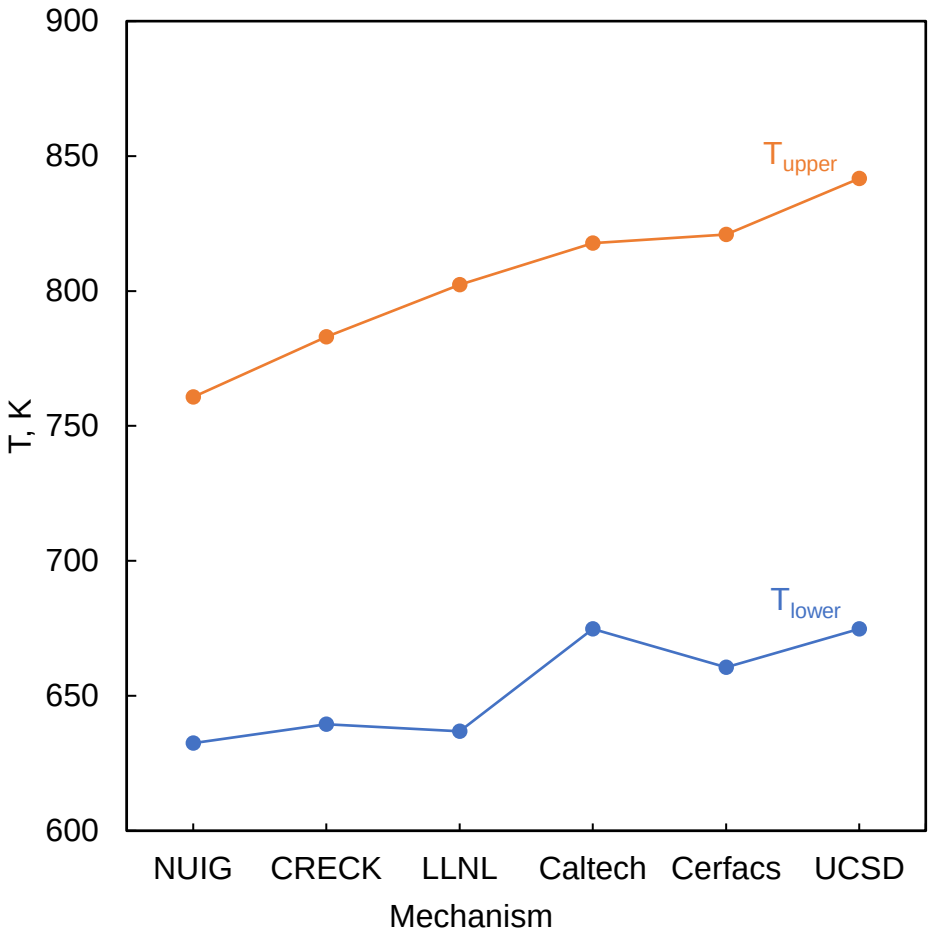

Figure 3.19. Lower and upper turnover temperatures for the six mechanisms outlined in Table 3.2. The blue line indicates the lower turnover temperature while the upper turnover temperature is denoted by the orange line

Table 3.3 represents the turnover temperature range ($T_{upper} - T_{lower}$) for all six mechanisms, calculated using the same cubic fitting method described in section 3.2, which utilizes a third-degree polynomial. It is clear that the chemical kinetic mechanism presented by the National University of Ireland, Galway (NUIG) has the narrowest NTC regime as compared to other five mechanisms.

Mechanism	**Turnover Range T_{upper} - T_{lower}, K**
CRECK	143.54
LLNL	165.49
NUIG	128.25
UCSD	166.94
CALTECH	142.95
CERFACS	160.41

Table 3.5. The turnover temperature range ($T_{upper} - T_{lower}$) for six mechanisms

Chapter 4: Conclusion and future work

As future internal combustion engines face more stringent demands for fuel efficiency, performance, and emissions, next-generation technologies are expected to use a variety of low temperature combustion processes that leverage cool flames, as outlined in chapter 1. Moreover, cool diffusion flames also play a critical role in process and fire safety.

In the present work, simulations of *n*-heptane autoignition using the Cantera code have led to several important discoveries, providing valuable insights into the behavior of cool diffusion flames:

- The autoignition of *n*-heptane unfolds in a two-stage process. It begins with a small temperature increase, which is then succeeded by a substantially larger increase. Remarkably, this phenomenon can be observed at atmospheric pressure when the starting temperatures of the mixture are between 450 – 775 K, extending its relevance beyond just high-pressure engine technologies.
- The cool flame phase is characterized by a notably lower heat release compared to the hot flame phase. With an increase in the initial mixture temperature, the rate of heat release during the cool flame phase progressively diminished until the cool flame phase disappeared entirely. This disappearance occurred at an initial mixture temperature beyond 775 K, indicating the maximum initial temperature limit for the existence of cool diffusion flames.
- The UCSD mechanism revealed a unique autoignition process unfolding in three distinct phases: Low-Temperature Ignition (LTI), Intermediate-Temperature Ignition (ITI), and High-Temperature Ignition (ITI). However, additional research

is needed to accurately quantify this behavior and understand its implications for engine technology.

- The two hydroperoxide species, Keto-hydroperoxide (KHP) and hydrogen peroxide (H_2O_2) play a critical role in the first and second stage ignition process, respectively. In the cool flame phase, only a portion of the fuel is utilized, aligning with the minimal heat release observed during this phase. Following this, the fuel undergoes complete oxidation in the hot ignition stage. During the cool flame phase, a limited amount of oxygen contributes to CO_2 formation, whereas the hot flame phase leads to a significant increase in CO_2 production. Furthermore, the investigation indicates that the cool flame phase is characterized by the generation of substantial quantities of formaldehyde and hydrogen peroxide.
- A unique region of non-monotonic mixture reactivity exists termed as the Negative – Temperature Coefficient (NTC) region that is fundamentally responsible for the existence of stable cool flames.
- A range for the NTC regime has been analyzed by determining the mean lower turnover temperature at 653 K and the mean upper turnover temperature at 804 K. Won et. al [19] measured flame temperature around 640 ± 30 K which is close to the modeled turnover temperature range. Similarly Farouk [58] measured a cool flame temperature of 700 K which also lies within the NTC range. Wadell et. al. [59] measured peak CDF temperatures of 705 and 760 K which also lies within the NTC range. Consequently, these modeled temperatures are in close agreement with experimentally measured temperatures as documented in the literature.

Additionally, this process also allows for the calculation of activation energy in both the low and high temperature region of the NTC curve.

- As fuel mixtures from lean to rich were investigated, the richer the fuel mixture, the shorter was the second-stage ignition delay time. The first-stage ignition delay time i.e., time to cool flame almost remains the same despite the mixture composition while the second-stage ignition delay time i.e. the hot flame phase is significantly affected by the mixture stoichiometry. A significant difference in ignition delay times can be observed within the NTC regime, i.e., between the lower and upper turnover thresholds.
- Six different chemical kinetic mechanisms were able to reproduce the NTC behavior and a turnover temperature range was established for the six mechanisms.

These simulations offer a wealth of data, opening avenues for extensive future research. While only *n*-heptane has been explored in this study, a wide range of hydrocarbon fuels are known to exhibit Negative Temperature Coefficient (NTC) behavior. This area of study, particularly focusing on heat release, two-stage ignition, low temperature combustion in the context of cool flames, remains largely unexplored for these fuels. Additionally, this investigative approach could be broadened to include other fuel components beyond standard hydrocarbons, such as traditional transportation fuels, renewable bio-derived fuels and many more offering the potential for identifying alternative fuels.

Secondly, the current understanding of cool flame chemistry is quite limited. It is also unknown which fuels can burn in air as cool diffusion flames. By utilizing these simulations across a range of initial mixture conditions and compositions, it becomes

possible to pinpoint the optimal conditions for sustaining stable cool diffusion flames. The insights gained from such data can help identify the temperature limits and mixture fractions for CDFs. This can help streamline the process of replicating and observing these flames in experimental setups, thereby conserving considerable time and resources. This can also help in characterizing flame temperatures, compositions, burning rates and emissions.

As these alternative fuels and conditions for existence of cool diffusion flames are identified, the broader goals of improving engine efficiency and reducing emissions can be achieved.

Appendix A: Cantera autoignition code

```
# Import necessary libraries
import pandas as pd
import numpy as np
import time
import cantera as ct

# Display the Cantera version being used
print(f"Running Cantera version: {ct.__version__}")

# Load the chemical mechanism for the gas
gas = ct.Solution(r"Mechanism_File_Path (.yaml File)")

# Set the initial reactor temperature and pressure
reactor_temperature = 825  # Temperature in Kelvin
reactor_pressure = 101325  # Pressure in Pascals (1 atm)

# Update the gas object with the reactor temperature and pressure
gas.TP = reactor_temperature, reactor_pressure

# Define the stoichiometry for the fuel/oxidizer mixture
gas.set_equivalence_ratio(phi=1, fuel="NC7H16", oxidizer={"O2": 1.0, "N2": 3.76})

# Initialize a batch reactor with the gas mixture and add it to a reactor network
r = ct.IdealGasConstPressureReactor(contents=gas, name="Batch Reactor")
reactor_network = ct.ReactorNet([r])

# Prepare a container to store the time history of the gas state
time_history = ct.SolutionArray(gas, extra="t")

def ignition_delay(states, species):
    """
    Function to compute the ignition delay based on the peak concentration of a given species.

    Parameters:
    states (SolutionArray): The states of the gas.
    species (str): The reference species to monitor.

    Returns:
    float: The ignition delay time in seconds.
    """
    i_ign = states(species).Y.argmax()
    return states.t[i_ign]
```

```
# Define the reference species for ignition delay calculation

reference_species = "oh"

# Start timing the simulation
t0 = time.time()

# Define an initial estimate for the ignition delay time (in seconds)
estimated_ignition_delay_time = 10

# Simulation start time
t = 0

# Counter for iteration steps
counter = 1
while t < estimated_ignition_delay_time:
    # Advance the simulation in time
    t = reactor_network.step()
    if not counter % 10:
        # Record the state every 10th step to reduce data size
        time_history.append(r.thermo.state, t=t)
    counter += 1

# Calculate the ignition delay using the specified reference species
tau = ignition_delay(time_history, reference_species)

# End timing the simulation
t1 = time.time()

# Print the computed ignition delay and the computation time
print(f"Computed Ignition Delay: {tau:.3e} seconds. Took {t1-t0:.2f}s to compute")

# Optionally, save the time history data to a CSV file
time_history.write_csv("Heptane_1_825.csv")
```

Appendix B: Temperature versus time plots

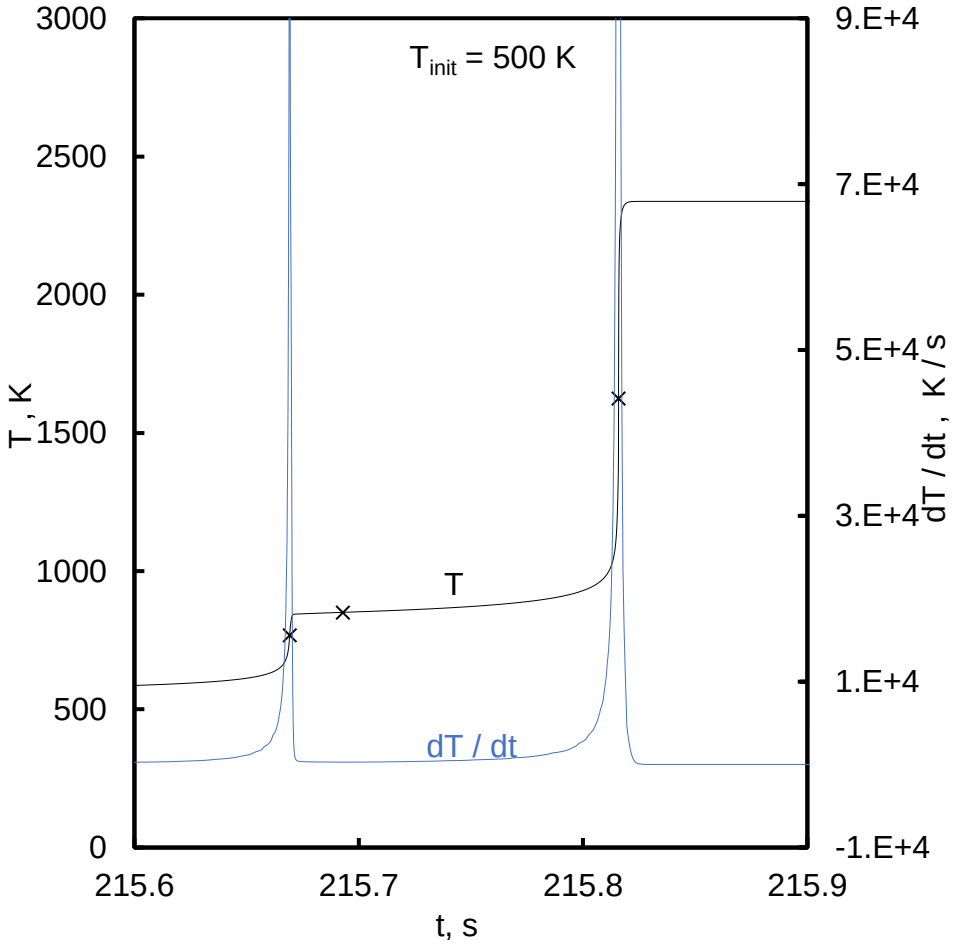

Figure B.1. Temperature versus time history for n-heptane/air mixture at atmospheric pressure and initial mixture temperature of 500 K

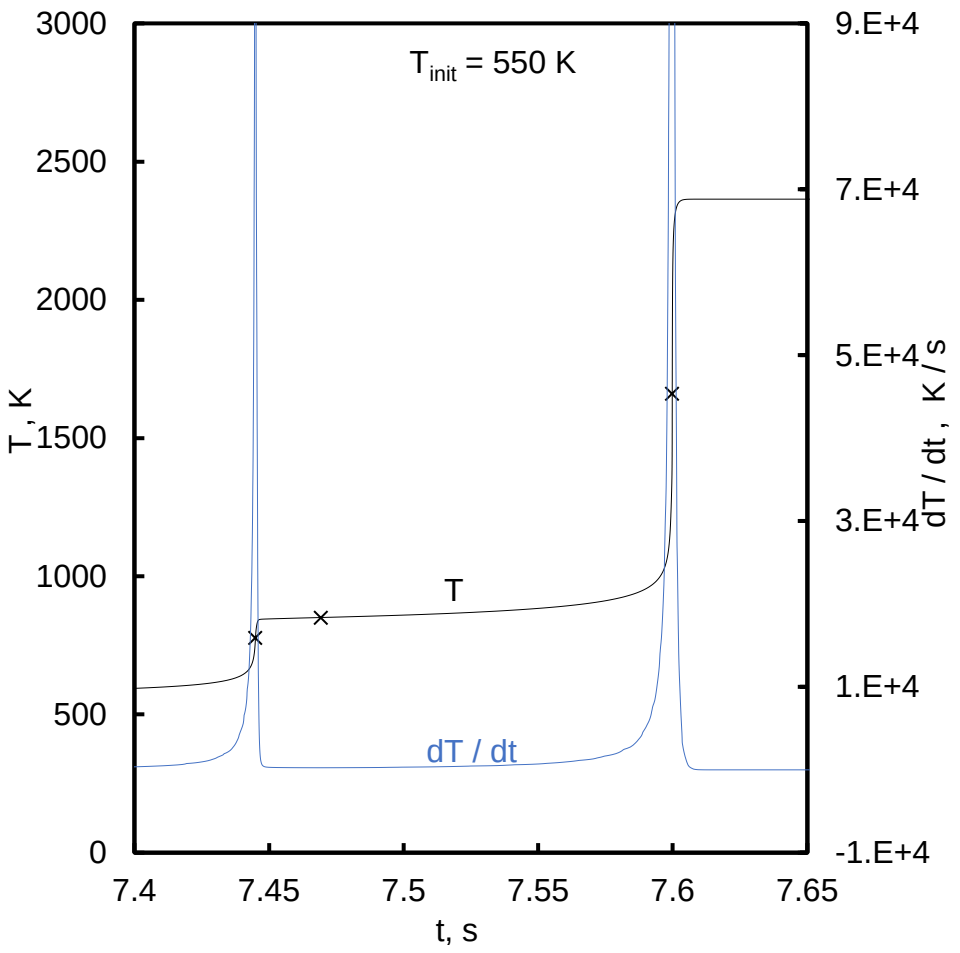

Figure B.2. Temperature versus time history for n-heptane/air mixture at atmospheric pressure and initial mixture temperature of 550 K

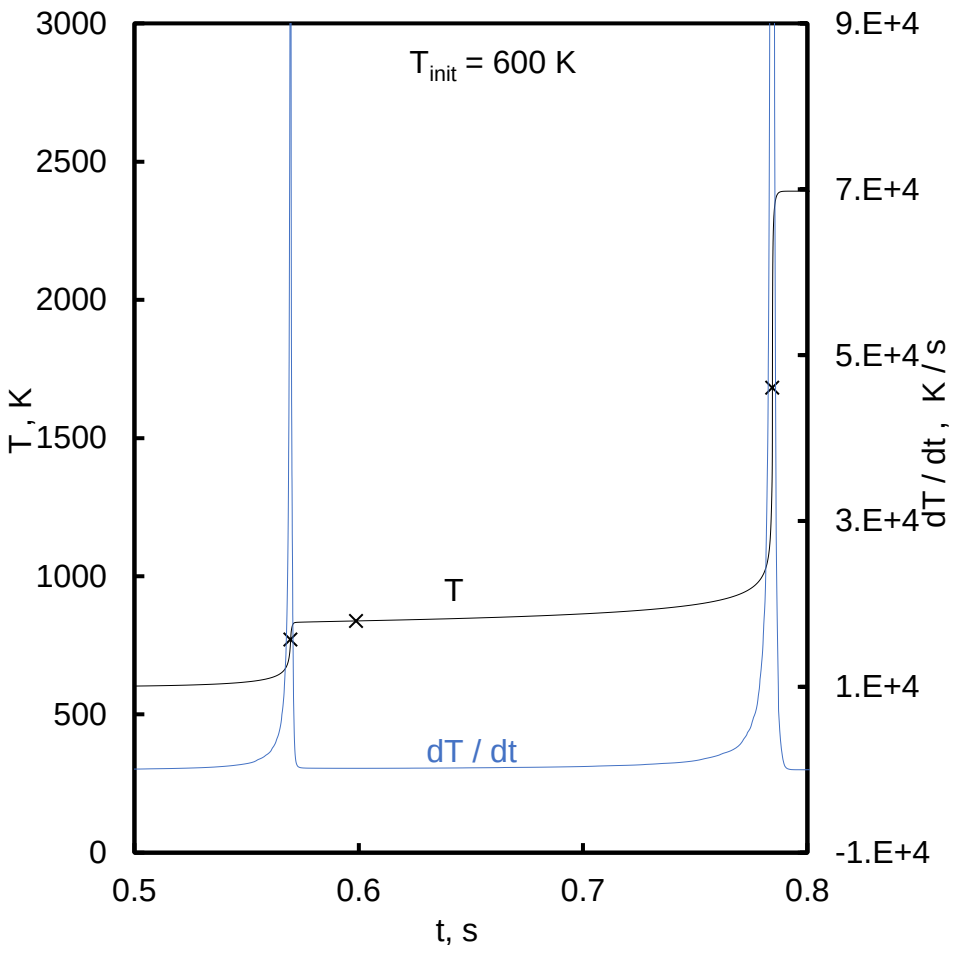

Figure B.3. Temperature versus time history for n-heptane/air mixture at atmospheric pressure and initial mixture temperature of 600 K

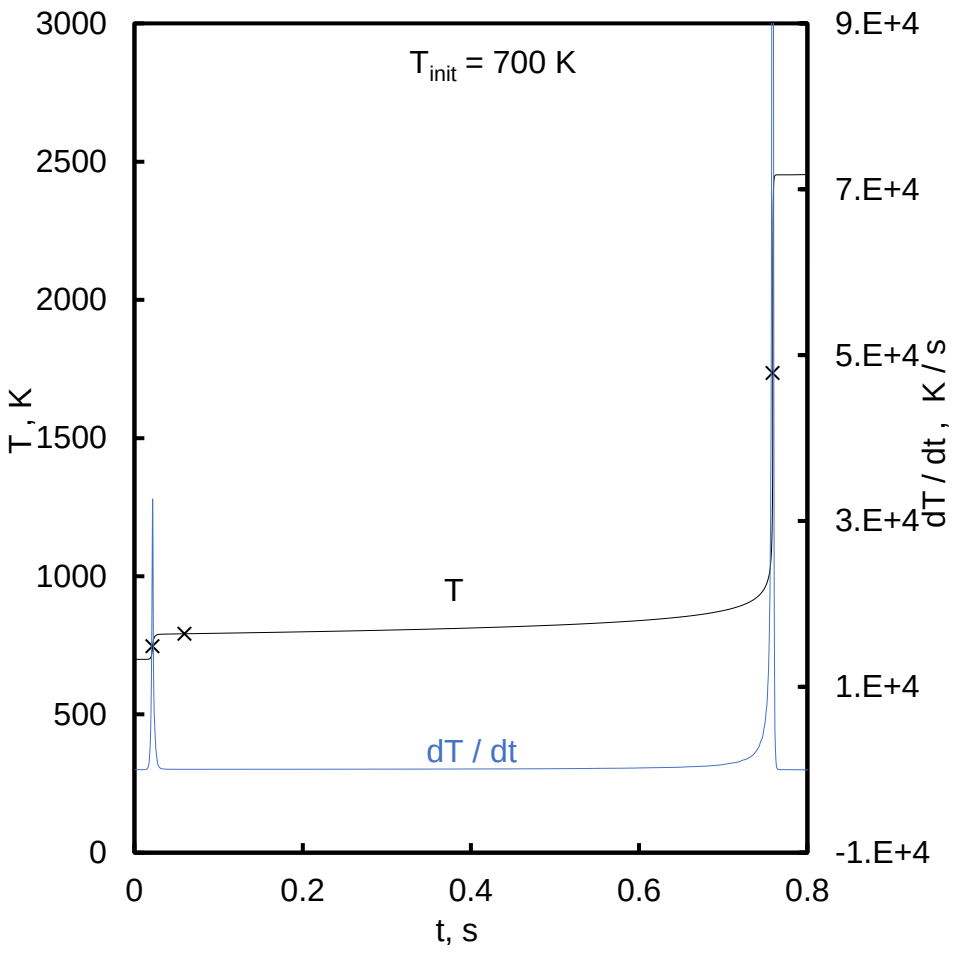

Figure B.4. Temperature versus time history for n-heptane/air mixture at atmospheric pressure and initial mixture temperature of 700 K

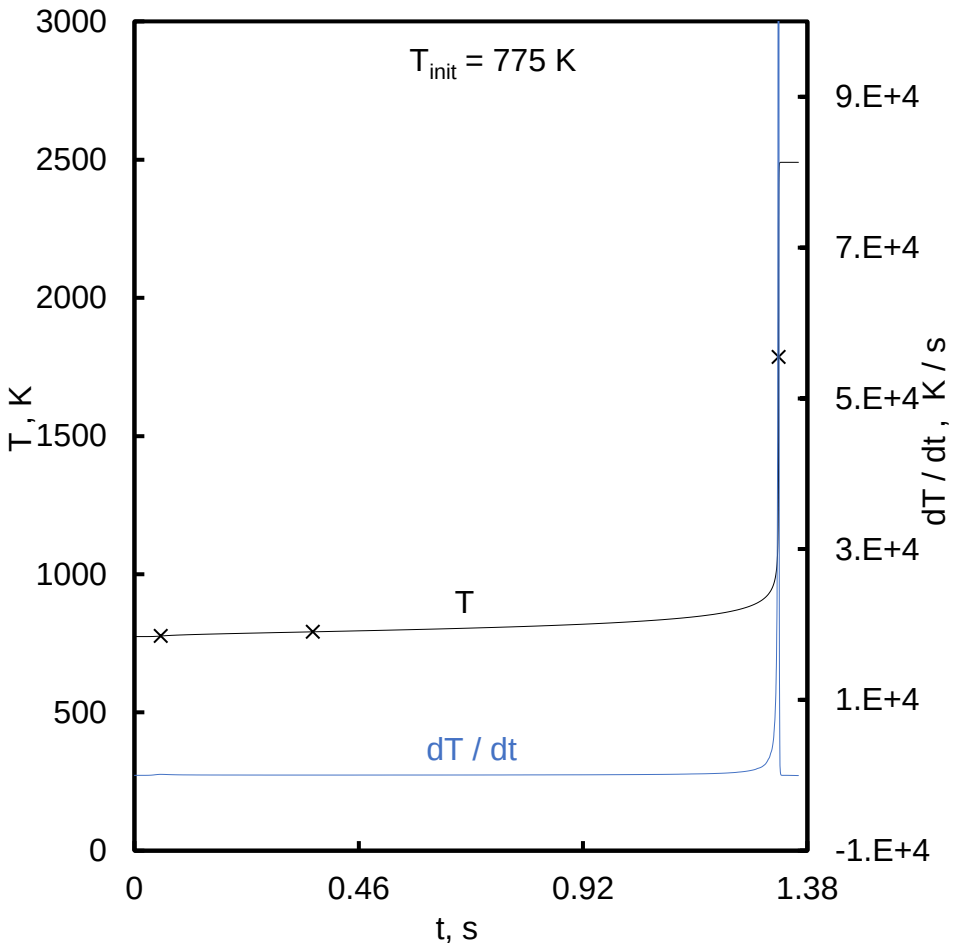

Figure B.5. Temperature versus time history for n-heptane/air mixture at atmospheric pressure and initial mixture temperature of 775 K

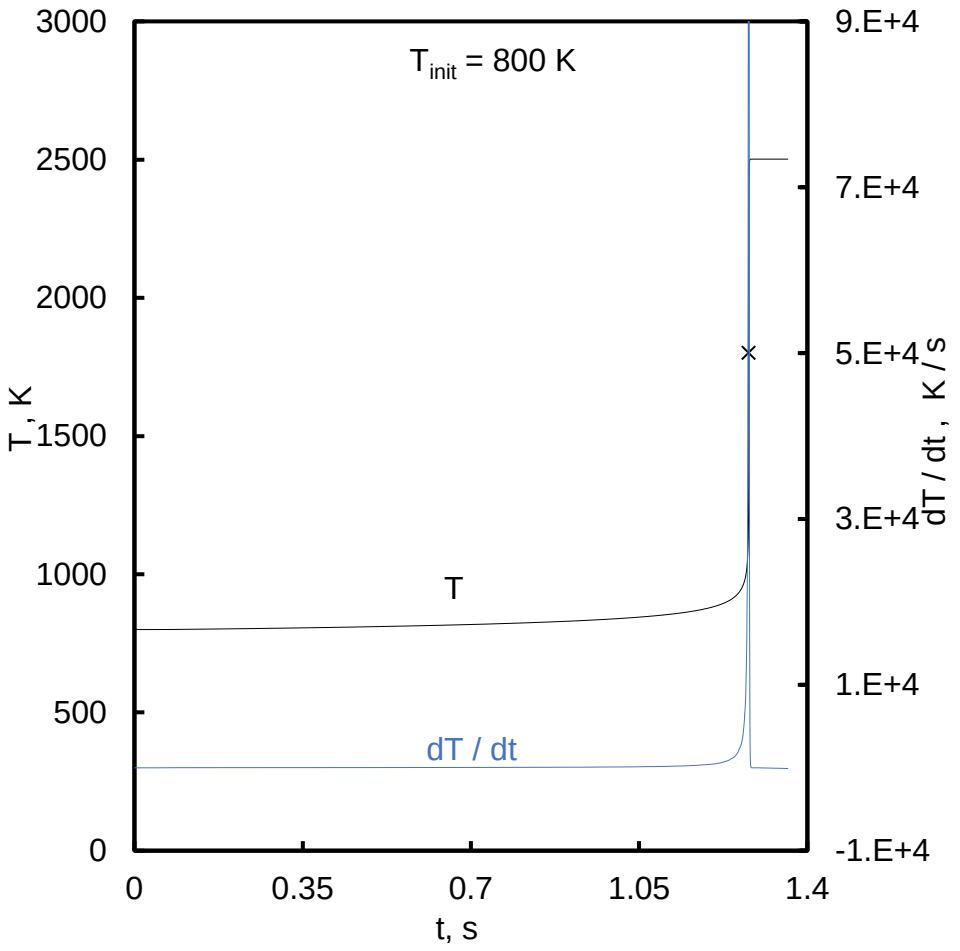

Figure B.6. Temperature versus time history for n-heptane/air mixture at atmospheric pressure and initial mixture temperature of 800 K

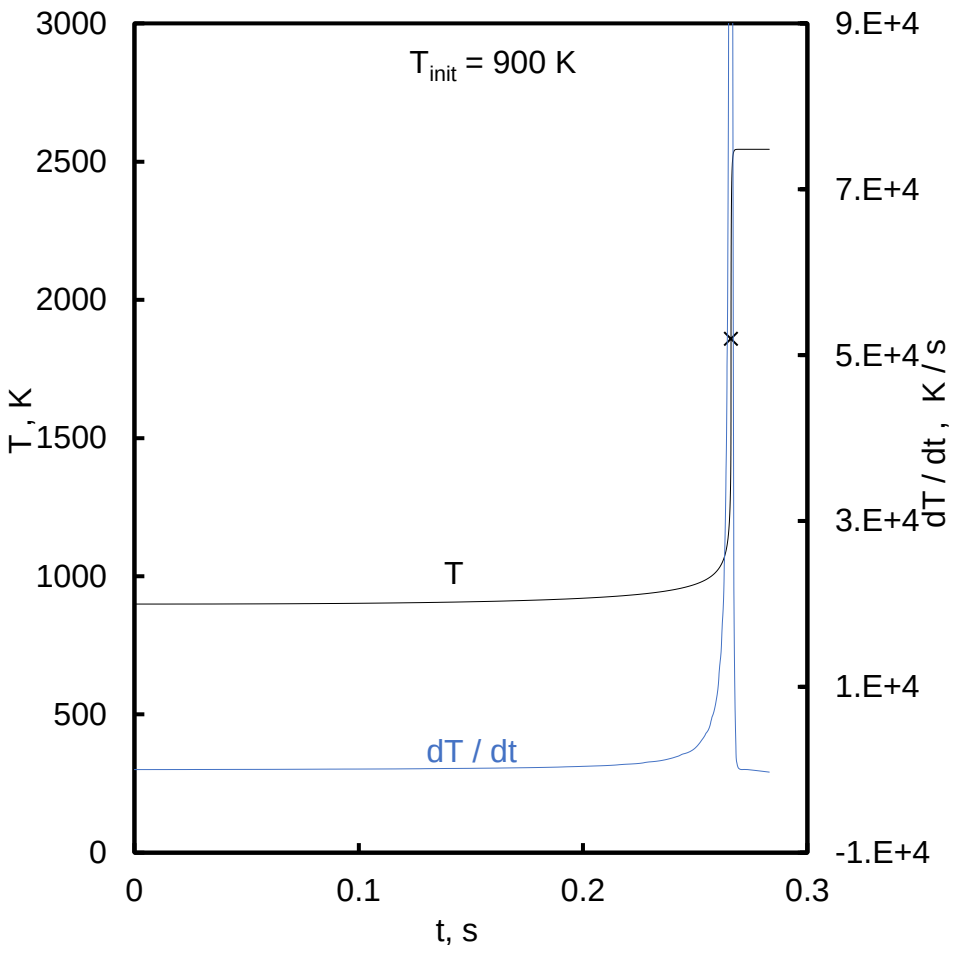

Figure B.7. Temperature versus time history for n-heptane/air mixture at atmospheric pressure and initial mixture temperature of 900 K

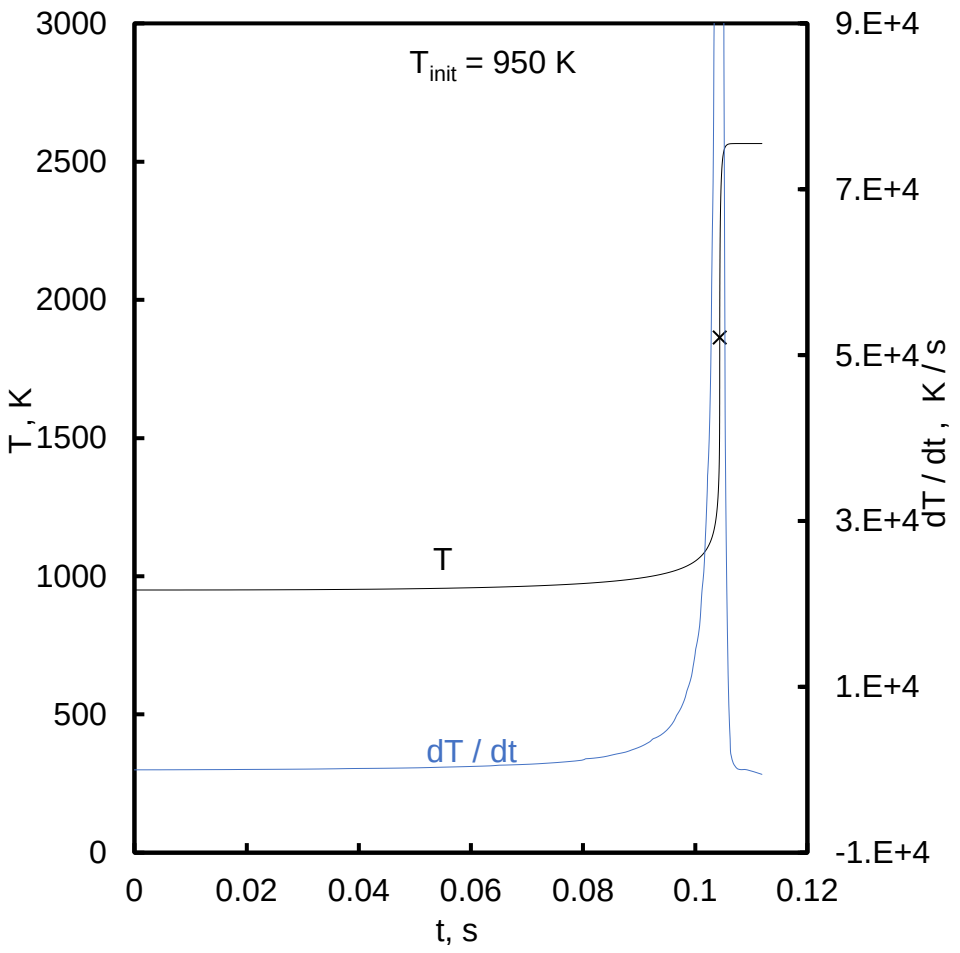

Figure B.8. Temperature versus time history for n-heptane/air mixture at atmospheric pressure and initial mixture temperature of 950 K

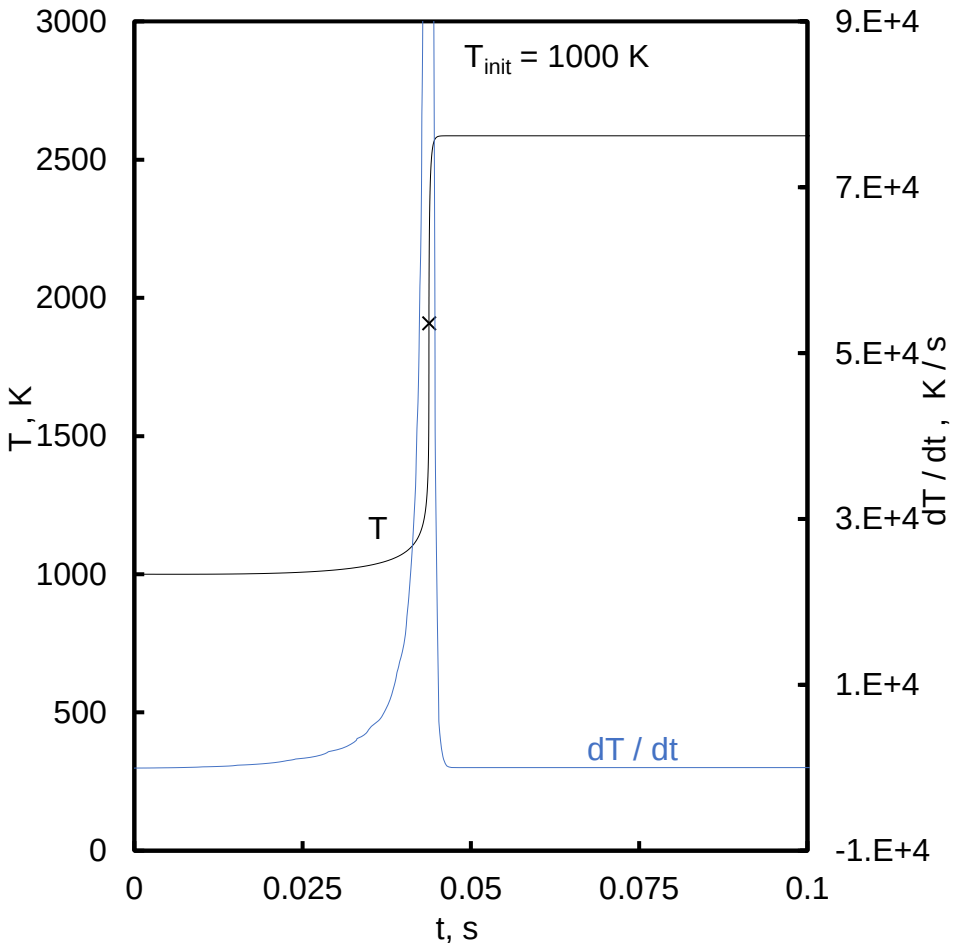

Figure B.9. Temperature versus time history for n-heptane/air mixture at atmospheric pressure and initial mixture temperature of 1000 K

References

[1] V. Nayagam, D. L. Dietrich, M. C. Hicks, and F. A. Williams, “Cool-flame extinction during n-alkane droplet combustion in microgravity,” *Combust. Flame*, vol. 162, no. 5, pp. 2140–2147, May 2015, doi: 10.1016/j.combustflame.2015.01.012.

[2] R. D. Reitz, “Directions in internal combustion engine research,” *Combust. Flame*, vol. 160, no. 1, pp. 1–8, Jan. 2013, doi: 10.1016/j.combustflame.2012.11.002.

[3] C. S. Yoo, T. Lu, J. H. Chen, and C. K. Law, “Direct numerical simulations of ignition of a lean n-heptane/air mixture with temperature inhomogeneities at constant volume: Parametric study,” *Combust. Flame*, vol. 158, no. 9, pp. 1727–1741, Sep. 2011, doi: 10.1016/j.combustflame.2011.01.025.

[4] M. Yao, Z. Zheng, and H. Liu, “Progress and recent trends in homogeneous charge compression ignition (HCCI) engines,” *Prog. Energy Combust. Sci.*, vol. 35, no. 5, pp. 398–437, Oct. 2009, doi: 10.1016/j.pecs.2009.05.001.

[5] T. Jin *et al.*, “Ignition dynamics of DME/methane-air reactive mixing layer under reactivity controlled compression ignition conditions: Effects of cool flames,” *Appl. Energy*, vol. 249, pp. 343–354, Sep. 2019, doi: 10.1016/j.apenergy.2019.04.161.

[6] G. R. Astbury, “Cool flames – laboratory curiosity or industrial hazard?,” no. 151, 2006.

[7] C. Arcoumanis, *Internal Combustion Engines*. Elsevier, 2012.

[8] J. B. Heywood, *Internal combustion engine fundamentals*, Second edition. New York: McGraw-Hill Education, 2018.

[9] Willard W. Pulkrabek, *Engineering Fundamentals of the Internal Combustion Engine*, Second.

[10] S. M. Sarathy, A. Farooq, and G. T. Kalghatgi, “Recent progress in gasoline surrogate fuels,” *Prog. Energy Combust. Sci.*, vol. 65, pp. 67–108, Mar. 2018, doi: 10.1016/j.pecs.2017.09.004.

[11] Z. Wang, H. Liu, and R. D. Reitz, “Knocking combustion in spark-ignition engines,” *Prog. Energy Combust. Sci.*, vol. 61, pp. 78–112, Jul. 2017, doi: 10.1016/j.pecs.2017.03.004.

[12] X. Zhen *et al.*, “The engine knock analysis – An overview,” *Appl. Energy*, vol. 92, pp. 628–636, Apr. 2012, doi: 10.1016/j.apenergy.2011.11.079.

[13] Y. Ju, “Understanding cool flames and warm flames,” *Proc. Combust. Inst.*, vol. 38, no. 1, pp. 83–119, 2021, doi: 10.1016/j.proci.2020.09.019.

[14] “Engineering Fundamentals of the Internal Combustion Engine.” Accessed: Feb. 17, 2024. [Online]. Available: https://www.pearson.com/en-us/subject-

catalog/p/engineering-fundamentals-of-the-internal-combustion-engine/P200000003345/9780131405707

[15] P. G. Lignola and E. Reverchon, “Cool flames,” *Prog. Energy Combust. Sci.*, vol. 13, no. 1, pp. 75–96, Jan. 1987, doi: 10.1016/0360-1285(87)90007-4.

[16] Y. Ju, C. B. Reuter, O. R. Yehia, T. I. Farouk, and S. H. Won, “Dynamics of cool flames,” *Prog. Energy Combust. Sci.*, vol. 75, p. 100787, Nov. 2019, doi: 10.1016/j.pecs.2019.100787.

[17] A. Cuoci, M. Mehl, G. Buzzi-Ferraris, T. Faravelli, D. Manca, and E. Ranzi, “Autoignition and burning rates of fuel droplets under microgravity,” *Combust. Flame*, vol. 143, no. 3, pp. 211–226, Nov. 2005, doi: 10.1016/j.combustflame.2005.06.003.

[18] V. Nayagam, D. L. Dietrich, P. V. Ferkul, M. C. Hicks, and F. A. Williams, “Can cool flames support quasi-steady alkane droplet burning?,” *Combust. Flame*, vol. 159, no. 12, pp. 3583–3588, Dec. 2012, doi: 10.1016/j.combustflame.2012.07.012.

[19] S. H. Won, B. Jiang, P. Diévart, C. H. Sohn, and Y. Ju, “Self-sustaining n - heptane cool diffusion flames activated by ozone,” *Proc. Combust. Inst.*, vol. 35, no. 1, pp. 881–888, 2015, doi: 10.1016/j.proci.2014.05.021.

[20] J. F. Griffiths and S. K. Scott, “Thermokinetic interactions: Fundamentals of spontaneous ignition and cool flames,” *Prog. Energy Combust. Sci.*, vol. 13, no. 3, pp. 161–197, Jan. 1987, doi: 10.1016/0360-1285(87)90010-4.

[21] G. Paczko, N. Peters, K. Seshadri, and F. A. Williams, “The role of cool-flame chemistry in quasi-steady combustion and extinction of *n*- heptane droplets,” *Combust. Theory Model.*, vol. 18, no. 4–5, pp. 515–531, Sep. 2014, doi: 10.1080/13647830.2014.934296.

[22] “Cool Flames - Perspectives on their importance in combustion systems.” Accessed: Feb. 21, 2024. [Online]. Available: https://www1.grc.nasa.gov/wp-content/uploads/Cool-Flames-Overview1.pdf

[23] C. H. Sohn, H. S. Han, C. B. Reuter, Y. Ju, and S. H. Won, “Thermo-kinetic dynamics of near-limit cool diffusion flames,” *Proc. Combust. Inst.*, vol. 36, no. 1, pp. 1329–1337, 2017, doi: 10.1016/j.proci.2016.05.049.

[24] A. Naidja, “Cool flame partial oxidation and its role in combustion and reforming of fuels for fuel cell systems,” *Prog. Energy Combust. Sci.*, vol. 29, no. 2, pp. 155–191, 2003, doi: 10.1016/S0360-1285(03)00018-2.

[25] F. Khaled, J. Badra, and A. Farooq, “Ignition delay time correlation of fuel blends based on Livengood-Wu description,” *Fuel*, vol. 209, pp. 776–786, Dec. 2017, doi: 10.1016/j.fuel.2017.07.095.

[26] J. E. Dec, “Advanced compression-ignition engines—understanding the in-cylinder processes,” *Proc. Combust. Inst.*, vol. 32, no. 2, pp. 2727–2742, 2009, doi: 10.1016/j.proci.2008.08.008.

[27] X. Lu, D. Han, and Z. Huang, “Fuel design and management for the control of advanced compression-ignition combustion modes,” *Prog. Energy Combust. Sci.*, vol. 37, no. 6, pp. 741–783, Dec. 2011, doi: 10.1016/j.pecs.2011.03.003.

[28] R. D. Reitz and G. Duraisamy, “Review of high efficiency and clean reactivity controlled compression ignition (RCCI) combustion in internal combustion engines,” *Prog. Energy Combust. Sci.*, vol. 46, pp. 12–71, Feb. 2015, doi: 10.1016/j.pecs.2014.05.003.

[29] D. K. Srivastava, A. K. Agarwal, A. Datta, and R. K. Maurya, Eds., *Advances in Internal Combustion Engine Research*. in Energy, Environment, and Sustainability. Singapore: Springer, 2018. doi: 10.1007/978-981-10-7575-9.

[30] A. A. Pekalski, J. F. Zevenbergen, H. J. Pasman, S. M. Lemkowitz, A. E. Dahoe, and B. Scarlett, “The relation of cool flames and auto-ignition phenomena to process safety at elevated pressure and temperature,” *J. Hazard. Mater.*, vol. 93, no. 1, pp. 93–105, Jul. 2002, doi: 10.1016/S0304-3894(02)00041-9.

[31] H. C. Lee, A. A. Mohamad, and L. Y. Jiang, “Comprehensive Comparison of Chemical Kinetics Mechanisms for Syngas/Biogas Mixtures,” *Energy Fuels*, vol. 29, no. 9, pp. 6126–6145, Sep. 2015, doi: 10.1021/acs.energyfuels.5b01136.

[32] “Supersonic Aircraft Fuel Tank Fire Hazard Investigation.” Accessed: Mar. 07, 2024. [Online]. Available: https://apps.dtic.mil/sti/citations/AD0847521

[33] “Analysis of Aircraft Fuel Tank Fire and Explosion Hazards.” Accessed: Mar. 07, 2024. [Online]. Available: https://apps.dtic.mil/sti/citations/AD0725027

[34] J. H. E. Cartwright, “Thermo-kinetic explosions: Safety first or safety last?,” *Phys. Fluids*, vol. 33, no. 3, p. 031401, Mar. 2021, doi: 10.1063/5.0037867.

[35] J. C. Livengood and P. C. Wu, “Correlation of autoignition phenomena in internal combustion engines and rapid compression machines,” *Symp. Int. Combust.*, vol. 5, no. 1, pp. 347–356, Jan. 1955, doi: 10.1016/S0082-0784(55)80047-1.

[36] “Petersengroup-IDT.” Accessed: Feb. 09, 2024. [Online]. Available: https://petersengroup.tamu.edu/research-2/gas-dynamics-chemical-kinetics/shock-tube-kinetics/idt/

[37] N. V. Petrukhin, N. N. Grishin, and S. M. Sergeev, “Ignition Delay Time − an Important Fuel Property,” *Chem. Technol. Fuels Oils*, vol. 51, no. 6, pp. 581–584, Jan. 2016, doi: 10.1007/s10553-016-0642-0.

[38] J. F. Griffiths, “REDUCED KINETIC MODELS AND THEIR APPLICATION TL-U PRACTICAL COMBUSTION SYSTEMS”.

[39] H. J. Curran, P. Gaffuri, W. J. Pitz, and C. K. Westbrook, “A Comprehensive Modeling Study of n-Heptane Oxidation,” *Combust. Flame*, vol. 114, no. 1–2, pp. 149–177, Jul. 1998, doi: 10.1016/S0010-2180(97)00282-4.

[40] M. Yoon, M. Choi, K. Kang, C. Oh, Y. Park, and G. Choi, “Effects of n-Heptane/Methane Blended Fuel on Ignition Delay Time in Pre-Mixed Compressed Combustion,” *Energies*, vol. 15, no. 11, p. 4081, Jun. 2022, doi: 10.3390/en15114081.

[41] “Cantera.” Accessed: Feb. 09, 2024. [Online]. Available: https://cantera.org/

[42] “Reactor Models in Cantera | Cantera.” Accessed: Feb. 09, 2024. [Online]. Available: https://cantera.org/science/reactors/reactors.html

[43] H. J. Curran, “Developing detailed chemical kinetic mechanisms for fuel combustion,” *Proc. Combust. Inst.*, vol. 37, no. 1, pp. 57–81, 2019, doi: 10.1016/j.proci.2018.06.054.

[44] N. Zettervall, C. Fureby, and E. J. K. Nilsson, “Evaluation of Chemical Kinetic Mechanisms for Methane Combustion: A Review from a CFD Perspective,” *Fuels*, vol. 2, no. 2, pp. 210–240, May 2021, doi: 10.3390/fuels2020013.

[45] S. S. Goldsborough, “A chemical kinetically based ignition delay correlation for iso-octane covering a wide range of conditions including the NTC region,” *Combust. Flame*, vol. 156, no. 6, pp. 1248–1262, Jun. 2009, doi: 10.1016/j.combustflame.2009.01.018.

[46] “CRECK_2003_TPRF_HT_LT_ALC - Creckmodeling.” Accessed: Feb. 09, 2024. [Online]. Available: https://creckmodeling.chem.polimi.it/menu-kinetics/menu-kinetics-detailed-mechanisms/107-category-kinetic-mechanisms/415-mechanisms-1911-tprf-ht-lt-alc/

[47] “n-Heptane Detailed Mechanism Version 3 | Combustion.” Accessed: Mar. 04, 2024. [Online]. Available: https://combustion.llnl.gov/mechanisms/alkanes/n-heptane-detailed-mechanism-version-3

[48] “Mechanism Downloads - University of Galway.” Accessed: Mar. 04, 2024. [Online]. Available: https://www.universityofgalway.ie/combustionchemistrycentre/mechanismdownloads/

[49] “Chemical Mechanism: Combustion Research Group at UC San Diego.” Accessed: Mar. 04, 2024. [Online]. Available: https://web.eng.ucsd.edu/mae/groups/combustion/mechanism.html

[50] “Explosion Dynamics Laboratory.” Accessed: Mar. 04, 2024. [Online]. Available: https://shepherd.caltech.edu/EDL/PublicResources/sdt/cti_mech.html

[51] “Jerzembeck detailed mechanism - CERFACS Chemistry.” Accessed: Mar. 04, 2024. [Online]. Available: https://chemistry.cerfacs.fr/en/chemical-database/mechanisms-list/jerzembecks-mechanism/

[52] E. Ranzi, A. Frassoldati, A. Stagni, M. Pelucchi, A. Cuoci, and T. Faravelli, “Reduced Kinetic Schemes of Complex Reaction Systems: Fossil and Biomass-Derived Transportation Fuels,” *Int. J. Chem. Kinet.*, vol. 46, no. 9, pp. 512–542, Sep. 2014, doi: 10.1002/kin.20867.

[53] W. Liang and C. K. Law, “Theory of first-stage ignition delay in hydrocarbon NTC chemistry,” *Combust. Flame*, vol. 188, pp. 162–169, Feb. 2018, doi: 10.1016/j.combustflame.2017.10.003.

[54] K. Zhang *et al.*, “An updated experimental and kinetic modeling study of n-heptane oxidation,” *Combust. Flame*, vol. 172, pp. 116–135, Oct. 2016, doi: 10.1016/j.combustflame.2016.06.028.

[55] J. C. Prince, F. A. Williams, and G. E. Ovando, “A short mechanism for the low-temperature ignition of n-heptane at high pressures,” *Fuel*, vol. 149, pp. 138–142, Jun. 2015, doi: 10.1016/j.fuel.2014.08.063.

[56] G. Blanquart, P. Pepiot-Desjardins, and H. Pitsch, “Chemical mechanism for high temperature combustion of engine relevant fuels with emphasis on soot precursors,” *Combust. Flame*, vol. 156, no. 3, pp. 588–607, Mar. 2009, doi: 10.1016/j.combustflame.2008.12.007.

[57] S. Jerzembeck, N. Peters, P. Pepiotdesjardins, and H. Pitsch, “Laminar burning velocities at high pressure for primary reference fuels and gasoline: Experimental and numerical investigation,” *Combust. Flame*, vol. 156, no. 2, pp. 292–301, Feb. 2009, doi: 10.1016/j.combustflame.2008.11.009.

[58] T. I. Farouk and F. L. Dryer, “Isolated n-heptane droplet combustion in microgravity: ‘Cool Flames’ – Two-stage combustion,” *Combust. Flame*, vol. 161, no. 2, pp. 565–581, Feb. 2014, doi: 10.1016/j.combustflame.2013.09.011.

[59] K. A. Waddell, H. J. Lee, V. Nayagam, R. L. Axelbaum, and P. B. Sunderland, “Cool diffusion flames in a stably stratified stagnation flow,” *Combust. Flame*, vol. 254, p. 112852, Aug. 2023, doi: 10.1016/j.combustflame.2023.112852.